

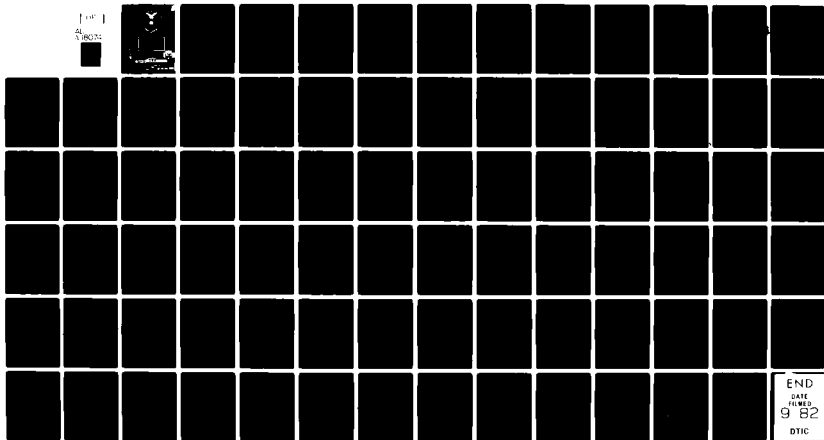
AD-A118 074

AIR FORCE INST OF TECH WRIGHT-PATTERSON AFB OH SCHOO--ETC F/6 18/3
A VARIATIONAL APPROACH TO THE RAYLEIGH-TAYLOR INSTABILITY OF AN--ETC(U)
DEC 81 J D TARGOVE
AFIT/6EP/PH/81D-11

UNCLASSIFIED

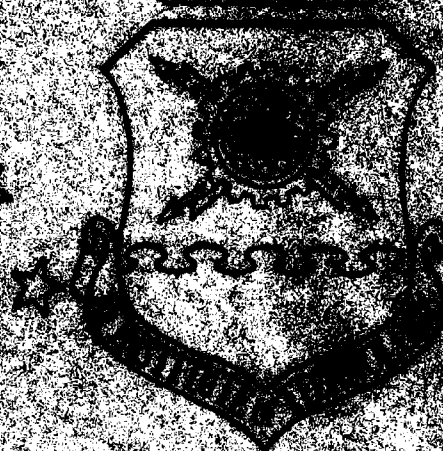
NL

AL 118 074
3 18C72



END
DATE
FILMED
9 82
DTIC

AD A118074



1

A VARIATIONAL APPROACH TO THE
RAYLEIGH-TAYLOR INSTABILITY OF AN
ACCELERATING PLASMA SLAB

THESIS

AFIT/GEP/PH/81D-11

James D. Targove
2nd Lt USAF

DTIC
S
AUG 11 1982
E

Approved for public release; distribution unlimited

A VARIATIONAL APPROACH TO THE RAYLEIGH-TAYLOR
INSTABILITY OF AN ACCELERATING PLASMA SLAB

THESIS

Presented to the Faculty of the School of Engineering
of the Air Force Institute of Technology
Air University
in Partial Fulfillment of the
Requirements for the Degree of
Master of Science

Accession For	
NTIS GRA&I	<input checked="checked" type="checkbox"/>
DTIC TAB	<input type="checkbox"/>
Unannounced	<input type="checkbox"/>
Justification	
By	
Distribution/	
Availability Codes	
Dist	Avail and/or Special
A	

by

James D. Targove, B.S.
2nd Lt USAF
Graduate Engineering Physics
December 1981



Acknowledgements

The topic for this work was suggested by Doctor Thomas Hussey of Sandia National Laboratory. Both he and Lt Col Norman Roderick of the Air Force Weapons Laboratory have been most helpful in providing information about actual implosions performed on the SHIVA and PROTO-II machines. I would also like to thank my thesis advisors, Lt Col John Erkkila and Major Michael Stamm, who have been extremely patient during my ramblings and have helped to guide this work.

Most importantly, I would like to thank my wife for putting up with my irregular hours and singlemindedness during this work.

James D. Targove

Contents

	<u>Page</u>
Acknowledgements	ii
List of Figures	iv
List of Tables	v
List of Symbols	vi
Abstract	viii
I. Introduction	1
The SHIVA Project	1
Scope	3
Assumptions	4
Organization	5
II. Background Theory	6
Application of the MHD Equations	6
Rayleigh-Taylor Instability.	12
A Continuous Density Transition	16
Linear Rayleigh-Ritz Method	18
III. Applications	21
Application of Rayleigh-Ritz Theory to the Hydromagnetic Problem	21
Approximate Forms for B and ρ	26
Growth Rates for a Plasma Sheath	30
IV. Results	36
Convergence of the Approximation	36
Instabilities with $\vec{k} \perp \vec{B}$	37
Oblique Perturbations	37
V. Conclusions	51
Bibliography	53
Appendix A: Cylindrical Sheath Implosion Relation	55
Appendix B: A Set of Orthonormal Functions	58
Appendix C: Evaluation of Needed Integrals	60
Vita	67

List of Figures

<u>Figure</u>		<u>Page</u>
1	Schematic of the Stages of a SHIVA Implosion	1
2	The Cylindrical Implosion Geometry and the Corresponding Planar Geometry	7
3	An Illustration of the Rayleigh-Taylor Instability	14
4	Example of the Class of Density Profiles Treated Here	18
5	A Linearly Decreasing Magnetic Field Profile	29
6	An Equilibrium Mass Density Corresponding to a Linear Magnetic Field	29
7	Growth Rate Estimates as a Function of Trial Function Length	41
8	Growth Rate Estimates as a Function of Perturbation Wavenumber	42
9	Growth Rate Estimates of Tsai et al for \vec{k} Perpendicular to \vec{B}	43
10	Growth Rate Estimates as a Function of Perturbation Wavenumber for True SHIVA Parameters and \vec{k} Perpendicular to \vec{B} Compared to the Growth Rates of LeLevier et al	44
11	Growth Rate Estimates as a Function of θ	45
12	θ_{marg} as a Function of Perturbation Wavenumber	46
13	Growth Rate Estimates as a Function of K_x for Constant K_y	47
14	Growth Rate Estimates of Tsai et al for \vec{k} Parallel to \vec{B}	48
15	Geometry of a Cylindrical Implosion	57

List of Tables

<u>Table</u>		<u>Page</u>
1	Simulation Data for a SHIVA Implosion . . .	49
2	Derived Quantities for a SHIVA Implosion . .	50

List of Symbols

k	Perturbation wavenumber
L	Magnetic diffusion penetration depth
u	x component of perturbed plasma velocity
V	y component of perturbed plasma velocity
w	z component of perturbed plasma velocity
z_0	z coordinate of density maximum
B	Magnetic field
B_0	Maximum magnetic field at boundary of plasma sheath
C_m, S_m	Orthonormal set of functions
D	$\frac{d}{dz}$
J	Current density
P_{mag}	Magnetic pressure
P_{mat}	Plasma material pressure
T	Dimensionless number related to magnetic tension
α_m, β_m	Adjustable Rayleigh-Ritz parameters
β	P_{mat}/P_{mag}
γ	Hydromagnetic instability growth rate
δ_{mn}	Kronnecker delta function
η	Electrical resistivity
θ	Angle between k and B
λ_m	Eigenvalue corresponding to C_m
λ_{th}	Sheath thickness
μ_m	Eigenvalue corresponding to S_m
ρ	Plasma mass density

List of Symbols (Contd)

σ Areal mass density

τ L/λ_{th}

Abstract

The growth rate of the hydromagnetic Rayleigh-Taylor instability is approximated here for an accelerating plasma slab. The slab is chosen as a large-radius approximation to an imploding cylindrical foil. A normal mode solution of the MHD equations is assumed, resulting in an integral relation for the instability growth rate. The Rayleigh-Ritz variational method is applied to the relation to estimate the growth rate. A linearly decreasing magnetic field is assumed in the slab perpendicular to the acceleration. A corresponding equilibrium mass density profile is then found. Growth rate estimates are then made for these profiles. Calculations are made for perturbation wavevectors perpendicular to the acceleration and at an angle θ to the magnetic field. The growth rates for $\theta = 90^\circ$ ^{4 degrees} compare favorably with LeLevier et al's results for a continuous density transition (14). Growth rates for $\theta = 0^\circ$ ^{4 degrees} are stable for all perturbation wavelengths and magnetic field strengths. This contradicts prior results in both slab and cylindrical geometry and suggests an error in this work.

I. Introduction

In this thesis the growth rates of the hydromagnetic Rayleigh-Taylor instability for an accelerating plasma slab are approximated using the Rayleigh-Ritz method. An accelerating slab is chosen as an approximation to an imploding cylindrical shell. Discussion of a current experimental effort points out the usefulness of this work.

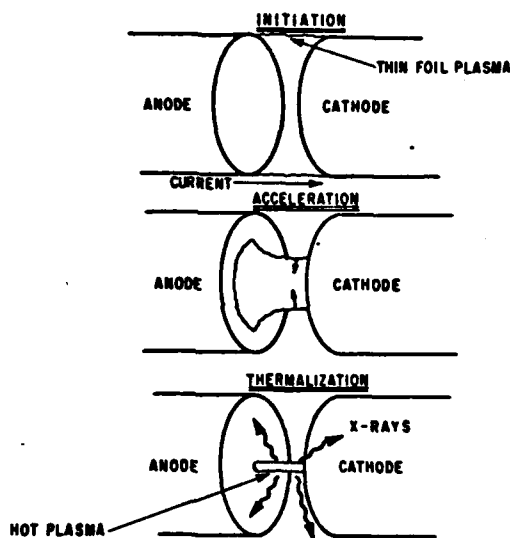


Figure 1. Schematic of the Stages of a SHIVA Implosion (20)

The SHIVA Project (4, 10, 11, 17)

The Air Force Weapons Laboratory is currently generating short, intense x-ray pulses with the SHIVA machine. SHIVA consists of a megajoule capacitor bank connected to a pair of electrodes. A thin (about one micron thick) cylindrical foil is placed between the electrodes. This

configuration is schematically illustrated in Figure 1. When the capacitor bank is switched across the electrodes the foil ionizes and expands into a plasma sheath. The mega-amp currents passing through the foil generate a mega-gauss azimuthal magnetic field outside of the foil. This external field is equivalent to that generated by a wire placed on axis:

$$B_{\theta} = \frac{2I}{r} \quad (1.1)$$

There is now a $\vec{J} \times \vec{B}$ force directed radially inward which causes the sheath to implode towards the axis. With the large current and magnetic field, the sheath obtains an average velocity on the order of 10^7 cm/sec as it collapses on axis. The sheath kinetic energy is then thermalized, producing a hot, dense plasma. This plasma radiates strongly in the x-ray region (see Figure 1). X-ray powers on the order of 10^{12} watts have already been observed.

Experience shows, however, that SHIVA performance in certain configurations is degraded by the presence of magnetohydrodynamic (MHD) instabilities. To see this, transform to the rest frame of the plasma sheath's center of mass. The plasma is then being accelerated against a magnetic pressure

$$P_m = \frac{B_{\theta}^2}{8\pi} \quad (1.2)$$

This is an unstable situation known as the hydromagnetic

Rayleigh-Taylor instability (13). This instability causes characteristic Rayleigh-Taylor ripples to grow along the outer plasma boundary. These ripples grow, and numerical simulations show that they can destroy the sheath if the wavelength of the ripples approaches the sheath thickness (17:274). This breakup in turn hinders the plasma thermalization by increasing the sheath thickness and therefore reduces the x-ray output. A good understanding of the Rayleigh-Taylor growth rates for the SHIVA implosion is therefore important.

Scope

This work is intended to approximate the Rayleigh-Taylor growth rates for the early part of the implosion, when the linear Rayleigh-Taylor instability dominates. Later in the implosion, the instability evolves into a non-linear stage which is more amenable to computer simulation (9). Growth rates for azimuthal perturbations are especially interesting since the current computer simulations operate in an r - z geometry only. The perturbations considered will have both z and θ variation. The effect of the azimuthal magnetic field as it diffuses into the plasma sheath will also be considered. This field acts to help stabilize the instability. This problem will be attacked here in a planar approximation with approximate forms for the magnetic field and plasma density profiles. These approximations should be good in the region of interest

near the outer edge of the sheath (where the instability occurs). Finally, these growth rates will be approximated using a variational technique (the Rayleigh-Ritz method) because an exact solution could not be found. An exact solution for the limiting case of z-axis perturbations has recently been reported by Tsai, Liskow, and Wilcox (19) for essentially the same planar problem. They also were forced to use numerical methods to handle azimuthal perturbations in the sheath, however.

Assumptions

All work here was done in planar geometry with a thin plasma sheath. Although the actual geometry is cylindrical, the agreement between the two geometries should be good during the early stages of the implosion. Cylindrical convergence effects are not yet significant (10), making a planar approximation acceptable.

Several assumptions are made about the sheath plasma itself. The sheath is assumed to be incompressible, to be describable by the ideal MHD equations, and to have zero electrical resistivity, all essentially for convenience. It should be mentioned, however, that a magnetic field cannot diffuse into an infinitely conducting plasma. Magnetic fields will therefore be frozen into the plasma sheath under the assumption that the fields would physically have diffused into the plasma and then have been frozen into place.

The next assumption is that the plasma viscosity is zero. Turchi and Baker state that for a typical SHIVA configuration the viscous Reynolds number exceeds 10^6 . The size of this quantity implies that viscosity can be ignored inside the sheath (20:4943).

Organization

The body of this work is organized as follows: In Chapter II the MHD equations are presented. These equations are linearized and a normal mode solution is assumed, resulting in an integral relation for the growth rates of the Rayleigh-Taylor instability. This relation cannot be solved exactly, so the Rayleigh-Ritz variational principle is presented as an approximate method of solution. Approximate forms for the magnetic field and plasma density profiles in the plasma sheath are developed in Chapter III for insertion into the integral relation. The Rayleigh-Ritz method is then applied to the integral relation to approximate the growth rates. To do this, a computer program was written. Its results are reported in Chapter IV.

This work is done in CGS-EMU units.

II. Background Theory

Application of the MHD Equations (2:48-56, 3:428-66)

The magnetohydrodynamic (MHD) model is one of the simplest models of a plasma available. It considers the plasma to be a single conducting fluid. In an ideal MHD model, the fluid is assumed to be infinitely conducting. This in turn implies local charge neutrality in the plasma. It is also assumed here that the fluid is incompressible and has no material viscosity.

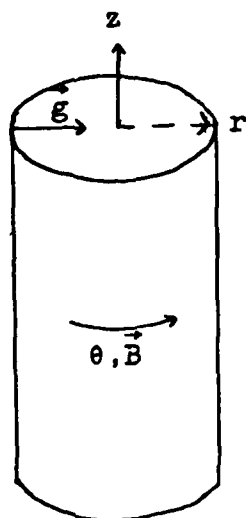
We wish here to model a plasma foil with a center of mass acceleration \vec{g} . It is therefore convenient to work in an accelerating reference frame moving with the plasma center of mass. A uniformly accelerating frame, the MHD equations, are identical to those in an inertial coordinate system except for the addition of a $+\rho\vec{g}$ force term to the equation of motion (19:1677). If the center of mass velocity is much less than the speed of light, which is certainly the case for an accelerating plasma, the current density \vec{J} and magnetic field \vec{B} have essentially the same magnitude in both the laboratory and plasma frames. The necessary MHD equations are then as follows:

1. The equation of motion

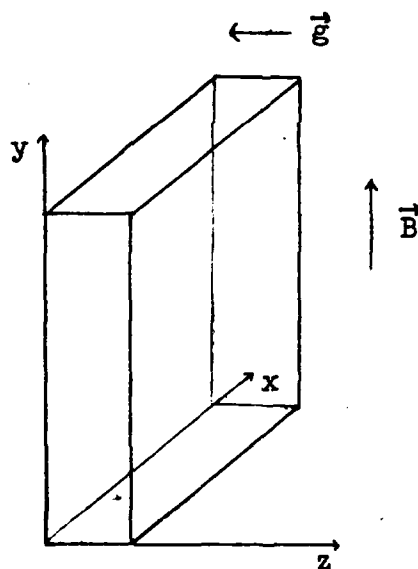
$$\rho \frac{d\vec{v}}{dt} = -\nabla P_{\text{mat}} + \frac{1}{c} \vec{J} \times \vec{B} + \rho\vec{g} \quad (2.1)$$

2. The incompressibility equation

$$\nabla \cdot \vec{v} = 0 \quad (2.2)$$



(a)



(b)

Figure 2. (a) The cylindrical implosion geometry in the lab frame. (b) The planar geometry under consideration in the rest frame of the plasma center of mass.

3. The mass continuity equation

$$\frac{\partial \rho}{\partial t} + \vec{V} \cdot \nabla \rho = 0 \quad (2.3)$$

and 4. Ampere's Law (with the displacement current ignored)

$$\nabla \times \vec{B} = \frac{4\pi}{c} \vec{J} \quad (2.4)$$

By inserting (2.4) into (2.1), using a vector identity for $(\nabla \times \vec{B}) \times \vec{B}$ and assuming that $\vec{B} \perp \nabla \vec{B}$, the Lorentz force can be replaced by

$$\begin{aligned} \frac{1}{c} \vec{J} \times \vec{B} &= -\nabla \frac{B^2}{8\pi} + \frac{1}{4\pi} \vec{B} \cdot \nabla \vec{B} \\ &= -\nabla P_{\text{mag}} + \frac{1}{4\pi} \vec{B} \cdot \nabla \vec{B} \end{aligned} \quad (2.5)$$

The Lorentz force therefore consists here of a pressure gradient component perpendicular to the magnetic field lines and a restoring force component opposing bending of the magnetic field lines. If the pressure P_{mat} in (2.1) is replaced by a total pressure $P = P_{\text{mat}} + P_{\text{mag}}$, (2.1) becomes

$$\rho \frac{d\vec{V}}{dt} = -\nabla P + \rho \vec{g} + \frac{1}{4\pi} \vec{B} \cdot \nabla \vec{B} \quad (2.6)$$

These equations are here applied to the geometry shown in Figure 2 with $\rho = \rho(z)$, $P = P(z)$, and $\vec{g} = -g\hat{z}$. The acceleration is, of course, not constant in a cylindrical implosion. The assumption here of a constant acceleration is equivalent to examining the sheath at one particular instant during the implosion. Acceleration in the $+z$

direction in Figure 2b corresponds to an acceleration in cylindrical coordinates in the $-r$ direction (see Figure 2a). Figure 2b therefore corresponds to an implosion in the positive z direction.

The equations (2.2), (2.3), and (2.6) are first linearized, with variables ϕ written as the sum of an equilibrium value ϕ_0 and a small perturbed value ϕ_1 which contains all the time dependence. The density pressure and velocity are therefore written as $\rho = \rho_0 + \rho_1$, $P = P_0 + P_1$, and $\vec{V} = \vec{V}_0 + \vec{V}_1$, respectively. From this point on the equilibrium values will be written without subscripts. When these forms for the variables are inserted into the equations, quadratic terms in perturbed quantities are ignored and time derivatives of equilibrium values equal zero. The equilibrium velocity $\vec{V}_0 = 0$ in the frame of the sheath.

A normal mode assumption is now made. All perturbed quantities ϕ_1 are assumed to have the form

$$\phi_1 = (\text{some function of } z) \cdot \exp(ik_x x + ik_y y + \gamma t) \quad (2.7)$$

dependence, with $k^2 = k_x^2 + k_y^2$. Any arbitrary perturbation can then be represented as a Fourier series of exponential terms. Only the fastest growing Fourier component is important, however. The simple dependence of (2.7) is therefore adequate here. Inserting the dependence in (2.7) into the linearized equations implies the substitutions

$$\frac{d}{dx} \rightarrow ik_x, \frac{d}{dy} \rightarrow ik_y, \text{ and } \frac{d}{dt} \rightarrow \gamma \quad (2.8)$$

The only remaining derivatives are with respect to z .

The details of the linearization and normal mode solution are carried out by Chandrasekhar (3:428-430, 457-466) for both the hydrodynamic and hydromagnetic cases (the non-conducting and conducting cases, respectively). In the hydrodynamic case the result is the differential equation

$$D(\rho Dw) - \rho k^2 w + \frac{k^2 g}{\gamma^2} (D\rho) w = 0 \quad (2.9)$$

where $D = \frac{d}{dz}$ and $w = V_z$. This equation is in Sturm-Liouville form. Sturm-Liouville theory states (3:432) that if $D\rho$ is positive everywhere, then all eigenvalues γ^2 are positive. If $D\rho$ is everywhere negative, all eigenvalues are negative. Finally, if $D\rho$ is anywhere positive then there exists at least one positive eigenvalue. The time dependence (2.7) means that an initial perturbation will grow exponentially if $\gamma^2 > 0$, resulting in an unstable state. If $\gamma^2 < 0$, the amplitude of a perturbation oscillates periodically, yielding a stable state. Combining these facts, we see that the configuration is unstable if $D\rho$ is positive anywhere, and it is stable if $D\rho$ is negative everywhere.

Adding the physical requirement that w must be continuous everywhere to (2.9), we see that if ρ and $D\rho$ are continuous then $D(\rho Dw)$ must also be continuous. This in

turn implies that Dw must also be continuous. Thus the continuity of ρ and $D\rho$ implies the continuity of w and Dw .

If ρ or $D\rho$ is discontinuous (say at $z = 0$), then a boundary condition can be derived by integrating (2.9) over an infinitesimal interval including $z = 0$. The result is

$$\Delta_0 (\rho Dw) = - \frac{k^2 g}{\gamma^2} (\Delta_0 \rho) w(0) \quad (2.10)$$

where $\Delta_0 \psi = \psi(0^+) - \psi(0^-)$.

For the hydromagnetic case with a magnetic field in the x - y plane equation (2.9) becomes (Ref 2:55)

$$\begin{aligned} D\left[\rho\gamma^2 + \frac{1}{4\pi} (\vec{k} \cdot \vec{B})^2\right] Dw \\ = k^2 \left[\rho\gamma^2 + \frac{1}{4\pi} (\vec{k} \cdot \vec{B})^2 - g D\rho\right] w \end{aligned} \quad (2.11)$$

This equation is more useful when transformed into a variational form. This is done by multiplying (2.11) by w and integrating both sides over some interval of interest (a,b) , giving

$$\begin{aligned} \int_a^b w D\left[\rho\gamma^2 + \frac{1}{4\pi} (\vec{k} \cdot \vec{B})^2\right] Dw \, dz \\ = k^2 \int_a^b w^2 \left[\rho\gamma^2 + \frac{1}{4\pi} (\vec{k} \cdot \vec{B})^2 - g D\rho\right] dz \end{aligned} \quad (2.12)$$

The left-hand side of (2.12) is then integrated by parts, assuming the boundary condition

$$w Dw \left[\rho\gamma^2 + \frac{1}{4\pi} (\vec{k} \cdot \vec{B})^2\right] \Big|_a^b = 0 \quad (2.13)$$

This condition is met in all cases considered here and (2.12) then becomes, after rearranging,

$$\frac{\gamma^2}{gk^2} = \frac{\int_a^b \{ (D\rho)w^2 - \frac{(\vec{k} \cdot \vec{B})^2}{4\pi} [(Dw)^2 + k^2 w^2] \} dz}{\int_a^b \rho \{ (Dw)^2 + k^2 w^2 \} dz} \quad (2.14)$$

This is the variational form which will be used here. Examination of (2.14) shows that it gives a real value for γ^2 if k is real (which it is here). Also, since the integral of the second numerator term in (2.14) is positive definite, we see that the growth rate decreases when a magnetic field is introduced with a component parallel to the perturbation wavevector k . This stabilization is due to the supporting magnetic pressure P_{mag} which helps to counter the plasma acceleration g . If $\vec{k} \perp \vec{B}$, the stabilizing term vanishes.

Rayleigh-Taylor Instability

The Rayleigh-Taylor instability is a macroscopic effect often encountered in hydrodynamics and hydromagnetics. It occurs when a more dense fluid is supported by a less dense fluid against a "downward" force. A classic example is a layer of water supported by a layer of oil against gravity. A small periodic perturbation along the fluid interface initially grows exponentially in amplitude. This growth can be explained with a simple energy argument. Figure 3 shows the perturbation. This perturbation involves the transfer of fluid from positive z to negative z regions.

This is an energetically favorable transfer. The perturbation will therefore grow. It has been shown experimentally (2:51) that this exponential growth changes into a linear growth with respect to time when the amplitude of the perturbation reaches about $2.5/k$. In this stage spikes of the heavier fluid fall and bubbles of the lighter fluid rise across the interface. Paradoxically the initial exponential growth is called the linear Rayleigh-Taylor instability while the linear growth stage is called the non-linear Rayleigh-Taylor instability (because the linear MHD equations no longer apply).

To show the linear instability analytically, consider the Sturm-Liouville equation (2.9). This equation has simple analytical solutions for two different density distributions. Rayleigh (15) showed that for an exponential density

$$\rho = \rho_0 e^{\beta z} \quad (2.15)$$

trapped between rigid walls at $z = 0$ and L , the velocity perturbation is of the form

$$w = A (e^{m_1 z} - e^{m_2 z}) \quad (2.16)$$

where m_1 and m_2 are the roots of

$$m^2 + m\beta - k^2 (1 - g\beta/\gamma^2) = 0 \quad (2.17)$$

with k , g , and γ having their previous meanings. The

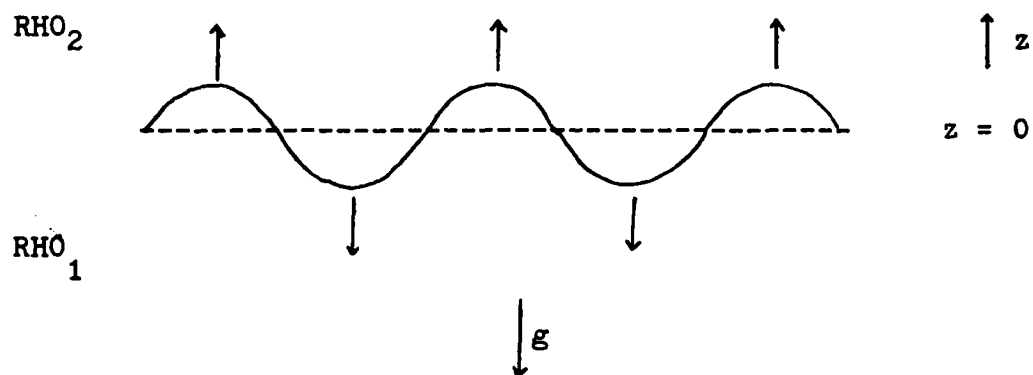


Figure 3. An illustration of the Rayleigh-Taylor instability mechanism.

instability growth rate is then the solution of the relation

$$\frac{g\beta}{\gamma^2} = 1 + \frac{\frac{1}{4} \beta^2 L^2 + \pi^2}{k^2 L^2} \quad (2.18)$$

Since the right-hand side of (2.18) is positive, γ^2 takes on the sign of β . The fluid is therefore stable for negative β and unstable for positive β .

Taylor (18) considered the stability of a discontinuous density of the form

$$\begin{aligned} \rho &= \rho_1, \quad z < 0 \\ &\rho_2, \quad z > 0 \end{aligned} \quad (2.19)$$

for constant ρ_1 and ρ_2 . Equation (2.9) then has a solution

$$\begin{aligned} w(z) &= Ae^{kz}, \quad z < 0 \\ &Ae^{-kz}, \quad z > 0 \end{aligned} \quad (2.20)$$

$\rho_1 < \rho_2$ is thus an unstable configuration, while $\rho_1 > \rho_2$ is stable.

This section has dealt so far only with the hydrodynamic case. There is a completely analogous effect in the hydromagnetic case in which the pressure P in (2.1) is replaced by a sum of plasma and magnetic pressures $P_{\text{mat}} + P_{\text{mag}}$. The nature of the instability is basically unchanged, however.

A Continuous Density Transition (14)

The linear growth rate estimates currently used in the SHIVA project are due to LeLevier, Lasher, and Bjorklund (14). They extended Taylor's treatment of a discontinuously stratified medium by assuming a continuous density transition of the form

$$\begin{aligned}\rho &= \rho_1 - \frac{1}{2} \delta\rho e^{-kz}, \quad z > 0 \\ \rho &= \rho_2 + \frac{1}{2} \delta\rho e^{kz}, \quad z < 0\end{aligned}\tag{2.22}$$

with $\delta\rho = \rho_1 - \rho_2 > 0$. Even for this relatively simple density distribution the differential equation (2.9) has no obvious analytical solution. LeLevier et al instead begin with the plasma equation of motion

$$\rho\dot{w} + D\rho + \rho g = 0\tag{2.23}$$

and the assumption

$$\rho_1 = -\int w D\rho dt\tag{2.24}$$

for the perturbed density. (2.23) and (2.24) are equivalent to the hydrodynamic equations (2.1) - (2.6) for $B = 0$.

A velocity perturbation of the form

$$\begin{aligned}w &= Af(t) \cos kx \exp(-kz), \quad z > 0 \\ w &= Af(t) \cos kx \exp(+kz), \quad z < 0\end{aligned}\tag{2.25}$$

is assumed, presumably because (2.25) is the simplest solution of the incompressibility condition

$$\nabla \cdot \vec{V} = 0 \quad (2.26)$$

in rectangular coordinates. (2.23) is then integrated over the intervals $(-\infty, 0)$ and $(0, \infty)$ using the velocity (2.25). This gives two expressions for the pressure at $z = 0$ which then are equated. Quadratic terms in f and \dot{f} are small and are dropped. The resulting equation is differentiated with respect to time to give

$$(\rho_1 + \rho_2) \ddot{f} - g \frac{kK}{k+K} \delta \rho f = 0 \quad (2.27)$$

The solution of this is

$$f(t) = \exp(\gamma t) \quad (2.28)$$

with

$$\gamma^2 = \frac{gkK \delta \rho}{(k+K)(\rho_1 + \rho_2)} \quad (2.29)$$

An interesting characteristic of this growth rate estimate is that γ remains finite for short wavelengths ($k \rightarrow \infty$). It also agrees well with numerical simulations of SHIVA implosions (17).

The assumed velocity (2.25) is not, however, consistent with the boundary condition (2.10) or the differential equation (2.9). There is no better choice, however, that satisfies the incompressibility condition (2.26). This problem has no obvious solution.

It should be mentioned that LeLevier et al have two sign errors in their report. First, the gravitational term in (2.23) has the wrong sign in their report. Second,

the provided velocity potential ϕ which leads to (2.25) by the relation $w = -D\phi$ requires a negative sign for the negative branch.

Linear Rayleigh-Ritz Method (6:193-206, 12:161-4)

The Rayleigh-Ritz method is a simple variational method used to approximate the eigenvalues of an ordinary differential equation. Only its application to the Sturm-Liouville equation

$$D(p Dw) - rw + \lambda sw = 0 \quad (2.30)$$

where p , r , s , and w are all functions of z and all eigenvalues are positive, will be discussed here.

As shown in Gelfand and Fomin (6:198), (2.30) can be expressed in the variational form

$$\lambda = \frac{\int_a^b (p(Dw)^2 + rw^2) dz}{\int_a^b sw^2 dz} \quad (2.31)$$

If both numerator and denominator are positive definite quantities, Rayleigh-Ritz theory states that the function w satisfying appropriate boundary conditions and minimizing λ in (2.31) is an eigenfunction of equation (2.30). This eigenfunction corresponds to the smallest eigenvalue of (2.30). This eigenvalue is then given by (2.31) with the eigenfunction substituted for w . Normally, however, this method is used only when the eigenfunctions cannot be found explicitly.

A trial function with adjustable parameters is used to approximate the eigenfunctions. In a linear Rayleigh-Ritz approximation, the trial function is of the form

$$w = \sum_{i=1}^q \alpha_i \phi_i(z) \quad (2.32)$$

where the ϕ 's are orthonormal functions satisfying the necessary boundary conditions. This trial function is now inserted into equation (2.31), giving an estimate of the eigenvalue. According to Rayleigh-Ritz theory (6), this estimate is greater than the true eigenvalue and converges monotonically to the eigenvalue as q increases.

The problem is now restated as that of minimizing

$$J(\alpha_1, \dots, \alpha_q) = \int_a^b (p(Dw)^2 + rw^2) dz \quad (2.33)$$

subject to the constraint

$$K(\alpha_1, \dots, \alpha_q) = \int_a^b sw^2 dz = 1 \quad (2.34)$$

This problem is identical to the original problem and in no way limits the class of allowable solutions (6). The new problem is solved using Lagrangian multipliers. Minimizing J subject to $K = 1$ therefore requires that

$$\frac{\partial}{\partial \alpha_i} (J - \sigma K) = 0, \quad i=1, \dots, q \quad (2.35)$$

where σ is an undetermined Lagrangian multiplier. (2.35)

is a system of q simultaneous linear equations. If J_{ij} and K_{ij} are defined such that

$$J = \sum_{i=1}^q \sum_{j=1}^q \alpha_i \alpha_j J_{ij} \quad (2.36)$$

and

$$K = \sum_{i=1}^q \sum_{j=1}^q \alpha_i \alpha_j K_{ij} \quad (2.37)$$

then the system will have a nontrivial solution if and only if

$$\det (D) = 0 \quad (2.38)$$

where

$$D_{ij} = J_{ij} - \sigma K_{ij} \quad (2.39)$$

σ is then the best estimate for the smallest eigenvalue λ_1 of (2.30) possible with the trial function (2.32) of order q . As the number of terms q in the trial function increases, the estimates decrease monotonically towards λ_1 as q goes to infinity.

The Rayleigh-Ritz method thus provides an upper bound on the first eigenvalue λ_1 of the Sturm-Liouville problem. The number of terms in the trial function can be increased until the accuracy of the approximation is sufficient.

III. Applications

Application of Rayleigh-Ritz Theory to the Hydromagnetic Problem

The Rayleigh-Ritz theory of Chapter II will here be applied to the variational equation (2.14) to estimate the growth rate γ for an accelerating plasma sheath. The sheath density will be assumed to peak in the center of the sheath with $D\rho > 0$ over $0 < z < z_0$ and $D\rho < 0$ for $z > z_0$ (see Figure 4).

The maximum growth rate might be expected with a trial velocity function w which is identically equal to zero for $z > z_0$. This assumption implies that there is no net plasma flow from the stable ($D\rho < 0$) into the unstable ($D\rho > 0$) region. As shown in Chapter II, Dw must be continuous everywhere if ρ is well behaved. Both $w(z_0)$ and $Dw(z_0)$ must therefore equal zero.

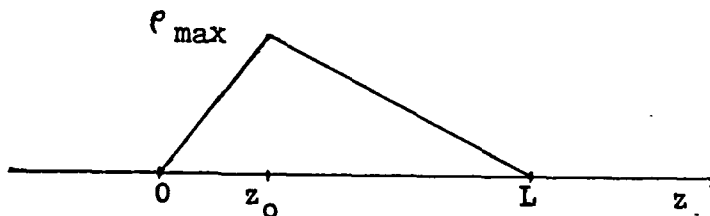


Figure 4. Example of the class of density profiles treated here.

An orthonormal set of functions is needed for the Rayleigh-Ritz procedure. The functions must be defined over the interval $(0, z_0)$ and meet the boundary conditions $w(z_0) = Dw(z_0) = 0$. Functions satisfying these conditions are

$$C_m \left(\frac{z}{z_0} - \frac{1}{2} \right) \text{ and } S_m \left(\frac{z}{z_0} - \frac{1}{2} \right)$$

where

$$C_m(u) = \frac{\cosh(\lambda_m u)}{\cosh(\lambda_m/2)} - \frac{\cos(\lambda_m u)}{\cos(\lambda_m/2)} \quad (3.1)$$

and

$$S_m(u) = \frac{\sinh(\mu_m u)}{\sinh(\mu_m/2)} - \frac{\sin(\mu_m u)}{\sin(\mu_m/2)} \quad (3.2)$$

C_m and S_m are discussed in Appendix B. They satisfy the boundary conditions

$$C_m \left(\pm \frac{1}{2} \right) = C'_m \left(\pm \frac{1}{2} \right) = S'_m \left(\pm \frac{1}{2} \right) = S_m \left(\pm \frac{1}{2} \right) = 0 \quad (3.3)$$

A satisfactory trial velocity function is

$$w(z) = \sum_{m=1}^q \alpha_m C_m \left(\frac{z}{z_0} - \frac{1}{2} \right) + \sum_{m=1}^q \beta_m S_m \left(\frac{z}{z_0} - \frac{1}{2} \right) \quad (3.4)$$

(3.4) also satisfies $w(0) = Dw(0) = 0$. These boundary conditions are equivalent to placing a rigid wall at $z = 0$. For lack of a better trial function, (3.4) will be used. Squaring (3.4),

$$w^2 = \sum_{m=1}^q \sum_{n=1}^q \left(\alpha_m C_m \left(\frac{z}{z_0} - \frac{1}{2} \right) + \beta_m S_m \left(\frac{z}{z_0} - \frac{1}{2} \right) \right) \cdot \left(\alpha_n C_n \left(\frac{z}{z_0} - \frac{1}{2} \right) + \beta_n S_n \left(\frac{z}{z_0} - \frac{1}{2} \right) \right) \quad (3.5)$$

Differentiating (3.4) and then squaring gives

$$(Dw)^2 = \frac{1}{z_0^2} \sum_{m=1}^q \sum_{n=1}^q (\alpha_m C_m' (\frac{z}{z_0} - \frac{1}{2}) + \beta_m S_m' (\frac{z}{z_0} - \frac{1}{2})) \cdot (\alpha_n C_n' (\frac{z}{z_0} - \frac{1}{2}) + \beta_n S_n' (\frac{z}{z_0} - \frac{1}{2})) \quad (3.6)$$

According to the linear Rayleigh-Ritz theory of Chapter II, the required equations are

$$\frac{\partial}{\partial \beta_m} (J - \lambda K) = 0 \quad m=1, \dots, q \quad (3.7)$$

and

$$\frac{\partial}{\partial \beta_m} (J - \lambda K) = 0 \quad m=1, \dots, q \quad (3.8)$$

where K and J are the numerator and denominator, respectively, of (2.14). λ is the Lagrangian multiplier.

Inserting (3.5) and (3.6) into (2.14), we obtain

$$\begin{aligned} J &= \int_0^{z_0} \rho ((Dw)^2 + k^2 w^2) dz \\ &= \int_0^{z_0} \rho \left\{ \frac{1}{z_0^2} \sum_{m=1}^q \sum_{n=1}^q (\alpha_m C_m' (\frac{z}{z_0} - \frac{1}{2}) + \beta_m S_m' (\frac{z}{z_0} - \frac{1}{2})) \cdot (\alpha_n C_n' (\frac{z}{z_0} - \frac{1}{2}) + \beta_n S_n' (\frac{z}{z_0} - \frac{1}{2})) \right. \\ &\quad \left. + k^2 \sum_{m=1}^q \sum_{n=1}^q (\alpha_m C_m (\frac{z}{z_0} - \frac{1}{2}) + \beta_m S_m (\frac{z}{z_0} - \frac{1}{2})) \cdot (\alpha_n C_n (\frac{z}{z_0} - \frac{1}{2}) + \beta_n S_n (\frac{z}{z_0} - \frac{1}{2})) \right\} dz \end{aligned} \quad (3.9)$$

Making the substitution

$$u = \frac{z}{z_0} - \frac{1}{2}$$

using the notation

$$(\phi_1|f|\phi_2) = \int \phi_1(u) f(u) \phi_2(u) du$$

and differentiating with respect to α_m ,

$$\begin{aligned} \frac{\partial J}{\partial \alpha_m} = \frac{2}{z_0} \sum_{n=1}^q \{ (\alpha_n (C_m' | \rho | C_n) + \beta_n (C_m' | \rho | S_n')) \\ + k^2 z_0^2 (\alpha_n (C_m | \rho | C_n) + \beta_n (C_m | \rho | S_n)) \} \end{aligned} \quad (3.10)$$

Noting the symmetry between C and S in (3.9), we can simply interchange α with β and C with S in (3.10) to obtain

$$\begin{aligned} \frac{\partial J}{\partial \beta_m} = \frac{2}{z_0} \sum_{n=1}^q \{ (\alpha_n (C_n' | \rho | S_m') + \beta_n (S_m' | \rho | S_n)) \\ + k^2 z_0^2 (\alpha_n (C_n | \rho | S_m) + \beta_n (S_m | \rho | S_n)) \} \end{aligned} \quad (3.11)$$

The function K will be subdivided into $K = K_1 - K_2$,
with

$$K_1 = \int_0^{z_0} (D\rho) w^2 dz \quad (3.12)$$

and

$$K_2 = \frac{\cos^2 \theta}{4\pi g} \int_0^{z_0} B^2 \{ (Dw)^2 + k^2 w^2 \} dz \quad (3.13)$$

Performing exactly the same operations on K_1 and K_2 as were performed on J gives

$$\frac{\partial K_1}{\partial \alpha_m} = 2z_0 \sum_{n=1}^q (\alpha_n (C_m | D\rho | C_n) + \beta_n (C_m | D\rho | S_n)) \quad (3.14)$$

$$\frac{\partial K_1}{\partial \beta_m} = 2z_0 \sum_{n=1}^q (\alpha_n (C_n | D\rho | S_m) + \beta_n (S_m | D\rho | S_n)) \quad (3.15)$$

$$\frac{\partial K_2}{\partial \alpha_m} = \frac{2 \cos^2 \theta}{4\pi g z_0} \sum_{n=1}^q \{ (\alpha_n (C_m | B^2 | C_n) + \beta_n (C_m | B^2 | S_n)) + k^2 z_0^2 (\alpha_n (C_m | B^2 | C_n) + \beta_n (C_m | B^2 | S_n)) \} \quad (3.16)$$

and

$$\frac{\partial K_2}{\partial \beta_m} = \frac{2 \cos^2 \theta}{4\pi g z_0} \sum_{n=1}^q \{ (\alpha_n (C_n | B^2 | S_m) + \beta_n (S_m | B^2 | S_n)) + k^2 z_0^2 (\alpha_n (C_n | B^2 | S_m) + \beta_n (S_m | B^2 | S_n)) \} \quad (3.17)$$

To simplify the final result, the relations (3.7) and (3.8) can be redefined as

$$\frac{\partial}{\partial \alpha_m} (J - \lambda K) = \sum_{n=1}^q (a_{mn} \alpha_n + b_{mn} \beta_n) = 0 \quad (3.18)$$

and

$$\frac{\partial}{\partial \beta_m} (J - \lambda K) = \sum_{n=1}^q (c_{mn} \alpha_n + d_{mn} \beta_n) = 0 \quad (3.19)$$

Once ρ and B have been inserted in (3.10), (3.11), and (3.14) - (3.17) the elements a_{mn} , b_{mn} , c_{mn} , and d_{mn} can be determined. With these new variables the equation to be satisfied is now in the block determinant form

$$\begin{vmatrix} A & B \\ C & D \end{vmatrix} = 0 \quad (3.20)$$

with A , B , C , and D being q by q matrices.

Once the matrix elements of (3.20) have been determined for a particular problem the values of λz_0 (a

dimensionless quantity) which solve (3.20) can be found as a function of k . Applying the Rayleigh-Ritz theory from Chapter II, we see that the growth rate estimate for (2.4) is

$$\frac{\gamma^2}{gk^2} \approx \frac{1}{\lambda_{\text{opt}}} \quad (3.21)$$

or

$$\gamma^2 = \frac{k^2 z_0^2}{\lambda_{\text{opt}} z_0} \frac{g}{z_0} \quad (3.22)$$

where the optimal root λ_{opt} is the smallest positive root of (3.20) or the largest negative one if there is no positive root. λ_{opt} therefore corresponds to the most unstable mode of the instability.

Approximate Forms for B and ρ

In a SHIVA implosion, the magnetic field is initially located totally outside the plasma sheath. The field then diffuses into the sheath according to the diffusion equation

$$\frac{\partial B}{\partial t} = \frac{\eta}{4\pi} \frac{\partial^2 B}{\partial z^2} \quad (3.23)$$

in a planar approximation, where η is the electrical resistivity. Hussey and Roderick (10) have shown that the external field B_0 increases linearly with time through much of the implosion time. This leads to a magnetic field profile

$$B(z, t) = 4 B_0(t) i^2 \operatorname{erfc} \left(\frac{z}{q} \right) \quad (3.24)$$

where

$$q = \left(\frac{nt}{\pi}\right) \quad (3.25)$$

and

$$i^2 \operatorname{erfc} \left(\frac{z}{q}\right) \quad (3.26)$$

is the second repeated integral of the complementary error function.

The greatest contribution to the instability growth rate comes from the outer edge of the plasma sheath where the plasma density rises quickly. For small z (3.26) is well approximated by (10)

$$B = B_0 \left(1 - \frac{4}{\pi^2} \frac{z}{q}\right) \quad (3.27)$$

where

$$q = 4.51 \lambda_{th} \quad (3.28)$$

for a sheath thickness λ_{th} . Sheath thickness is here defined as sheath mass per unit area divided by maximum sheath density.

The linear magnetic field (3.27) equals zero when

$$z = \frac{q\pi}{4} = 2 \lambda_{th} \quad (3.29)$$

This small z approximation will be extended throughout the whole plasma sheath under the assumption that the small- z region determines the instability of the sheath. The magnetic profile used here is therefore

$$B(z) = B_0 \left(1 - \frac{z}{L}\right) \quad (3.30)$$

where $L = 2\lambda_{th}$. This profile is illustrated in Figure 5.

Hussey, Roderick, and Kloc (11:1454-5) have used the equilibrium equation of motion

$$\rho g = - \frac{\partial}{\partial z} (P_{mat} + P_{mag}) \quad (3.31)$$

to derive an equilibrium density distribution which corresponds to the linear magnetic field profile (3.30). This density distribution is (see Figure 6)

$$\begin{aligned} \rho &= 2\bar{\rho} \left(1 + \beta - \frac{z}{L} - (1+\beta) \exp \left(-\frac{z}{\beta L} \right) \right), \quad 0 < z < L \\ &2\bar{\rho} \left(\beta - (1+\beta) \exp \left(-\frac{1}{\beta} \right) \right) \exp \left(\frac{L-z}{\beta L} \right), \quad z > L \end{aligned} \quad (3.32)$$

where $\bar{\rho}$ is an average sheath density and

$$L = \frac{P_{mat}}{P_{mag}} \quad (3.33)$$

is defined in terms of the maximum magnetic pressure and the average plasma pressure. Differentiating ρ with respect to z shows that the peak density occurs at

$$z = z_0 = \beta L \ln \left(\frac{1+\beta}{\beta} \right) \quad (3.34)$$

and is

$$\rho_{max} = 2\bar{\rho} \left(1 - \beta \ln \left(\frac{1+\beta}{\beta} \right) \right) \quad (3.35)$$

For small values of β , very little plasma is located in the region $z > L$. The plasma is therefore concentrated in a region twice the defined sheath thickness.

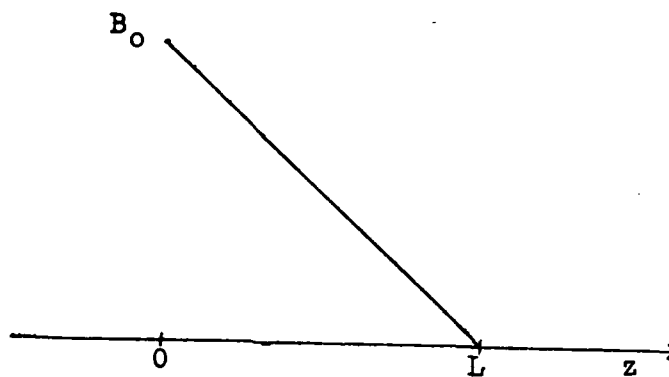


Figure 5. A linearly decreasing magnetic field profile.

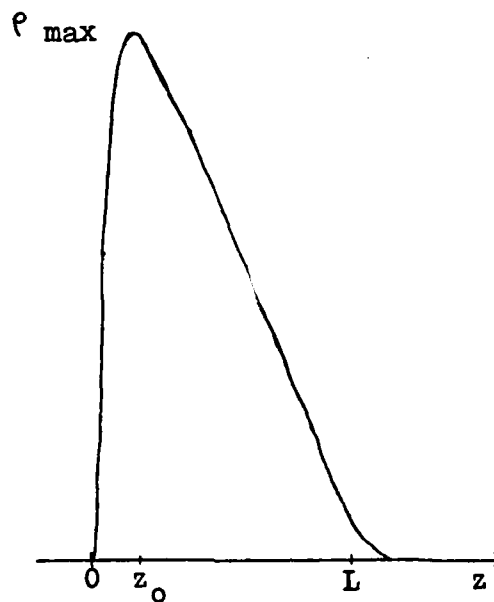


Figure 6. An equilibrium mass density corresponding to a linear magnetic field.

Growth Rates for a Plasma Sheath

Growth rates for the Rayleigh-Taylor instability in an accelerating plasma sheath are addressed in this section. This development is the major result of this work.

The density distribution

$$\rho = 2\bar{\rho} \left\{ (1+\beta) - \frac{z}{L} - (1+\beta) \exp \left(-\frac{z}{\beta L} \right) \right\} \quad (3.35a)$$

for $0 < z < L$ will be used here, along with the magnetic field

$$B(z) = B_0 \left(1 - \frac{z}{L} \right) \quad (3.36a)$$

(3.35a) and (3.35b) need only be inserted into the equations (3.10) - (3.17). The determinant equation (3.20) will then be solved, giving the desired growth rate estimate.

If the density (3.35a) is inserted into (3.10) we get

$$\begin{aligned} \frac{\partial J}{\partial \alpha_m} = & \frac{4\bar{\rho}}{z_0} \left(1 + \beta - \frac{z_0}{2L} \right) \sum_{n=1}^q \{ (\alpha_n (C_m' | C_n') + \beta_n (C_m' | S_n')) \\ & + k^2 z_0^2 (\alpha_n (C_m | C_n) + \beta_n (C_m | S_n)) \} \\ & - \frac{4\bar{\rho}}{L} \sum_{n=1}^q \{ (\alpha_n (C_m' | u | C_n') + \beta_n (C_m' | u | S_n')) \\ & + k^2 z_0^2 (\alpha_n (C_m | u | C_n) + \beta_n (C_m | u | S_n)) \} \\ & - \frac{4\bar{\rho}(1+\beta)}{z_0} \exp \left(-\frac{z_0}{2\beta L} \right) \\ & \cdot \sum_{n=1}^q \{ (\alpha_n (C_m' | \exp(-\frac{z_0 u}{\beta L}) | C_n') + \beta_n (C_m' | \exp(-\frac{z_0 u}{\beta L}) | S_n')) \\ & + k^2 z_0^2 (\alpha_n (C_m | \exp(-\frac{z_0 u}{\beta L}) | C_n) + \beta_n (C_m | \exp(-\frac{z_0 u}{\beta L}) | S_n)) \} \end{aligned} \quad (3.36)$$

Orthonormality yields

$$(C_m | C_n) = \delta_{mn} \text{ and } (C_m | S_n) = 0$$

while parity considerations mean that

$$(C_m' | S_n') = (C_m' | u | C_n') = (C_m | u | C_n) = 0$$

Inserting these values into (3.36) gives

$$\begin{aligned} \frac{\partial J}{\partial \alpha_m} = & \frac{4\bar{\rho}}{z_0} \left(1 + \beta - \frac{z_0}{2L}\right) \sum_{n=1}^q \alpha_n ((C_m' | C_n') + k^2 z_0^2 \delta_{mn}) \\ & - \frac{4\bar{\rho}}{L} \sum_{n=1}^q \beta_n ((C_m' | u | S_n') + k^2 z_0^2 (C_m | u | S_n)) \\ & - \frac{4\bar{\rho}(1+\beta)}{z_0} \exp\left(-\frac{z_0}{2\beta L}\right) \\ & \cdot \sum_{n=1}^q \{ \alpha_n ((C_m' | \exp(-\frac{z_0 u}{\beta L}) | C_n') + k^2 z_0^2 (C_m | \exp(-\frac{z_0 u}{\beta L}) C_n)) \\ & + \beta_n ((C_m' | \exp(-\frac{z_0 u}{\beta L}) | S_n') + k^2 z_0^2 (C_m | \exp(-\frac{z_0 u}{\beta L}) S_n)) \} \end{aligned} \quad (3.36a)$$

Noting the symmetry between C and S in (3.9), we can simply interchange α with β and C with S in (3.36a) to obtain

$$\begin{aligned} \frac{\partial J}{\partial \beta_m} = & \frac{4\bar{\rho}}{z_0} \left(1 + \beta - \frac{z_0}{2L}\right) \sum_{n=1}^q \beta_n ((S_m' | S_n') + k^2 z_0^2 \delta_{mn}) \\ & - \frac{4\bar{\rho}}{L} \sum_{n=1}^q \alpha_n ((C_n' | u | S_m') + k^2 z_0^2 (C_n | u | C_m)) \\ & - \frac{4\bar{\rho}(1+\beta)}{z_0} \exp\left(-\frac{z_0}{2\beta L}\right) \end{aligned}$$

$$\begin{aligned}
& \cdot \sum_{n=1}^q \{ \beta_n ((S_m | \exp(-\frac{z_0 u}{\beta L}) | S_n) + k^2 z_0^2 (S_m | \exp(-\frac{z_0 u}{\beta L}) | S_n)) \\
& + \alpha_n ((C_n | \exp(-\frac{z_0 u}{\beta L}) | S_m) + k^2 z_0^2 (C_n | \exp(-\frac{z_0 u}{\beta L}) | S_n)) \} \quad (3.37)
\end{aligned}$$

Inserting

$$D_p = 2\bar{\rho} \left\{ -\frac{1}{L} + \frac{1+\beta}{\beta L} \exp(-\frac{z}{\beta L}) \right\} \quad (3.38)$$

into (3.14) and (3.15) yields

$$\begin{aligned}
\frac{\partial K_1}{\partial \alpha_m} &= \frac{4\bar{\rho} z_0}{L} \left\{ -\alpha_m + \frac{1+\beta}{\beta} \exp(-\frac{z_0}{2\beta L}) \right. \\
& \cdot \sum_{n=1}^q (\alpha_n (C_m | \exp(-\frac{z_0 u}{\beta L}) | C_n) + \beta_n (C_m | \exp(-\frac{z_0 u}{\beta L}) | S_n)) \} \\
& \quad (3.39)
\end{aligned}$$

and

$$\begin{aligned}
\frac{\partial K_1}{\partial \beta_m} &= \frac{4\bar{\rho} z_0}{L} \left\{ -\beta_m + \frac{1+\beta}{\beta} \exp(-\frac{z_0}{2\beta L}) \right. \\
& \cdot \sum_{n=1}^q (\beta_n (S_m | \exp(-\frac{z_0 u}{\beta L}) | S_n) \\
& \quad + \alpha_n (C_n | \exp(-\frac{z_0 u}{\beta L}) | S_m)) \} \quad (3.40)
\end{aligned}$$

Inserting the B field (3.30) into (3.16) and (3.17) yields

$$\begin{aligned}
\frac{\partial K_2}{\partial \alpha_m} &= \frac{2B_0^2 z_0 \cos^2 \theta}{4\pi g L^2} \sum_{n=1}^q \{ \alpha_n ((C_m | u^2 | C_n) + k^2 z_0^2 (C_m | u^2 | C_n) \\
& + (\frac{L}{z_0} - \frac{1}{2})^2 ((C_m | C_n) + \delta_{mn} k^2 z_0^2)) \\
& - \beta_n (\frac{2L}{z_0} - 1) ((C_m | u | S_n) + k^2 z_0^2 (C_m | u | S_n)) \} \quad (3.41)
\end{aligned}$$

and

$$\begin{aligned}
\frac{\partial K_2}{\partial \beta_m} = & \frac{2B_0^2 z_0 \cos^2 \theta}{4\pi g L^2} \sum_{n=1}^q \{ \beta_n ((S'_m | u^2 | S'_n) + k^2 z_0^2 (S_m | u^2 | S_n)) \\
& + (\frac{L}{z_0} - \frac{1}{2})^2 ((S'_m | S'_n) + k^2 z_0^2 \delta_{mn}) \} \\
& - \alpha_n (\frac{2L}{z_0} - 1) ((C'_n | u | S'_m) + k^2 z_0^2 (C_n | u | S_m)) \} \quad (3.42)
\end{aligned}$$

The expressions (3.36) - (3.42) can now be substituted into (3.18) and (3.19) to give values for the matrix elements a' through d' , where

$$a'_{mn} = \frac{L}{\rho} a_{mn} \quad (3.43)$$

and so on for b , c , and d . The results are then

$$\begin{aligned}
a'_{mn} = & \frac{4}{\tau} (1 + \beta - \frac{\tau}{2}) (C'_m | C'_n) \\
& - \frac{4(1+\beta)}{\tau} \exp(-\frac{\tau}{2\beta}) ((C'_m | \exp(-\frac{\tau u}{\beta}) | C'_n) \\
& + k^2 z_0^2 (C_m | \exp(-\frac{\tau u}{\beta}) | C_n)) \\
& - 4\tau\lambda L (\frac{1+\beta}{\beta}) \exp(-\frac{\tau}{2\beta}) (C_m | \exp(-\frac{\tau u}{\beta}) | C_n) \\
& + 2\tau\lambda L (k^2 z_0^2 (C_m | u^2 | C_n) + (C'_m | u^2 | C'_n) \\
& + (\frac{1}{\tau} - \frac{1}{2})^2 (C'_m | C'_n)) \\
& + \delta_{mn} (\frac{4}{\tau} (1 + \beta - \frac{\tau}{2}) k^2 z_0^2 + 4\tau\lambda L + 2\tau\lambda L (\frac{1}{\tau} - \frac{1}{2})^2 k^2 z_0^2) \quad (3.44)
\end{aligned}$$

$$\begin{aligned}
b'_{mn} = c'_{nm} = & -4 \{ (C'_m | u | S'_n) + k^2 z_0^2 (C_m | u | S_n) \} \\
& - \frac{4(1+\beta)}{\tau} \exp \left(-\frac{\tau}{2\beta} \right) \{ (C'_m | \exp \left(-\frac{\tau u}{\beta} \right) | S'_n) + k^2 z_0^2 (C_m | \exp \left(-\frac{\tau u}{\beta} \right) | S_n) \} \\
& - 4\tau\lambda L \left(\frac{1+\beta}{\beta} \right) \exp \left(-\frac{\tau}{2\beta} \right) (C_m | \exp \left(-\frac{\tau u}{\beta} \right) | S_n) \\
& - 2\tau T \lambda L \left(\frac{2}{\tau} - 1 \right) \{ k^2 z_0^2 (C_m | u | S_n) + (C'_m | u | S'_n) \} \quad (3.45)
\end{aligned}$$

and

$$\begin{aligned}
d'_{mn} = & \frac{4}{\tau} (1+\beta - \frac{\tau}{2}) (S'_m | S'_n) \\
& - \frac{4(1+\beta)}{\tau} \exp \left(-\frac{\tau}{2\beta} \right) \{ (S'_m | \exp \left(-\frac{\tau u}{\beta} \right) | S'_n) \\
& \quad + k^2 z_0^2 (S_m | \exp \left(-\frac{\tau u}{\beta} \right) | S_n) \} \\
& - 4\tau\lambda L \left(\frac{1+\beta}{\beta} \right) \exp \left(-\frac{\tau}{2\beta} \right) (S_m | \exp \left(-\frac{\tau u}{\beta} \right) | S_n) \\
& + \delta_{mn} \left\{ \frac{4k^2 z_0^2}{\tau} (1+\beta - \frac{\tau}{2}) + 4\tau\lambda L + 2\tau T \lambda L k^2 z_0^2 \left(\frac{1}{\tau} - \frac{1}{2} \right)^2 \right\} \quad (3.46)
\end{aligned}$$

with

$$\tau = \frac{z_0}{L} \quad (3.47)$$

and

$$T = \frac{B_0^2 \cos^2 \theta}{4\pi g L \rho} \quad (3.48)$$

If the substitution

$$g = \frac{B_0^2}{8\pi \rho L} \quad (3.49)$$

is made, then (3.48) becomes

$$T = 2 \cos^2 \theta \quad (3.50)$$

All matrix elements of the equation

$$\begin{vmatrix} A' & B' \\ C' & D' \end{vmatrix} = 0 \quad (3.51)$$

are now known. From the first section of this chapter, the eigenvalues λ of this equation allow an estimate of the growth rate

$$2 = \frac{k^2 L^2}{\lambda_{opt} L} \frac{g}{L} \quad (3.52)$$

or

$$\frac{\gamma^2 L}{g} = \frac{k^2 z_0^2}{\lambda_{opt} L \tau^2} \quad (3.53)$$

A FORTRAN program was written to solve (3.51) for λ as a function of $k^2 z_0^2$, θ , and β . The results of the program are discussed in Chapter IV. All the unevaluated integrals in (3.44) - (3.46) are evaluated in Appendix C.

IV. Results

The Rayleigh-Ritz approximation to the hydromagnetic instability growth rates of an accelerating plasma sheath was developed in Chapter III. A computer program was written to implement the approximation. The results of this approximation are presented here. The stabilizing effects of a magnetic field diffused into the sheath are also discussed.

Parameters needed for the approximation are provided by a one-dimensional simulation to the SHIVA implosion using the MAGPIE code. The simulation data at selected times is listed in Table 1. This raw data is converted into necessary parameters in Table 2. The necessary relations to generate these parameters are given in Appendix A.

Convergence of the Approximation

As the number of terms in the trial velocity w increases, the growth rate approximation provided by the procedure of Chapter III should converge to the actual growth rate. This is illustrated in Figure 7 for several cases with perturbation wavevector $\vec{k} \perp \vec{B}$. For these cases the growth rate estimates increase by 25 to 30 percent as the trial function increases from 2 to 4 terms. The growth rates increase by just 1 to 2 percent as the trial function increases from 18 to 20 terms. The convergence seems to be rather slow.

Instabilities with $\vec{k} \perp \vec{B}$

The limiting case of a perturbation $\vec{k} \perp \vec{B}$ will be discussed here. This planar case is equivalent to a cylindrical instability with only z-axis perturbations. In cylindrical coordinates it is just the sausage instability.

Figure 8 shows the resulting dispersion relation for typical plasma parameters. We see that the sheath is unstable for all wavelengths of perturbation, approaching zero for long wavelengths and an upper limit for the growth rate as $\lambda \rightarrow 0$ ($k \rightarrow \infty$). This upper limit is not evident in the figure, but it was verified for extremely small wavelengths ($k z_0 \approx 10^3$). This general behavior agrees with that of Tsai, Liskow, and Wilcox for basically the same problem (Figure 9).

The dimensionless growth rates of Figure 8 are transformed into actual growth rates in Figure 10 for several times during the SHIVA implosion. The data from Table 2 has been used, with the β rounded to the nearest multiple of .05. The solid lines in Figure 10 represent growth rate estimates made using LeLevier's result for an exponentially transitioning density. It is assumed here that LeLevier's density scale length $1/K = z_0/4\pi$. The agreement between the two methods is then excellent (within 5 percent).

Oblique Perturbations

Perturbations with wavevectors not perpendicular to \vec{B} were considered. Figure 11 shows growth rates for a

constant perturbation wavelength as the angle θ between \vec{k} and \vec{B} decreases from 90° . As the wavevector rotates, the destabilizing perpendicular component decreases while the stabilizing parallel component increases (parallel and perpendicular will hereafter be with respect to \vec{B}). There therefore exists an angle θ_{marg} at which marginal stability is achieved. This θ_{marg} is an overestimate which also converges to the true value as the length of the trial function increases.

The variation of θ_{marg} with perturbation wavelength and the number of trial function terms is illustrated in Figure 12. We see that θ_{marg} increases moderately as perturbation wavelength decreases. Even though the unstabilized perpendicular instability is greater for larger wavenumbers, the stabilizing influence of the parallel instability grows even faster with k . Stability therefore occurs at smaller angles as k increases.

In Figure 13 the perpendicular component of the perturbation wavevector k_x remains constant while the parallel component k_y is increased. In this case the destabilizing effect of k_x is held constant while the stabilizing influence of k_y is gradually increased until a value $(k_y)_{\text{marg}}$ is reached at which the two effects cancel out to yield marginal stability. Figure 13 shows that long-wavelength parallel components can be used to stabilize much shorter-wavelength perpendicular components λ_x , with the growth

rate being linear in k_y . This stabilization causes the growth rates to decrease when a long-wavelength component is introduced. This fact is especially important when the problem is related to cylindrical geometry. The stabilizing θ -perturbation wavelengths of a cylindrical sheath are on the order of the cylinder radius for low-order modes while the destabilizing z -perturbation wavelengths are on the order of the sheath thickness. This suggests that long-wavelength θ perturbations might be able to largely stabilize the z instabilities.

These results, however, disagree with previous work done on this problem. Tsai, Liskow, and Wilcox (19) have recently reported the dispersion relation for parallel perturbations shown in Figure 14. The sheath becomes unstable for long wavelength perturbations, with a mode of maximum instability existing approximately midway between the two points of marginal stability. These unstable modes were not observed here, however.

— Experimental evidence also supports the belief that unstable modes exist for long wavelength perturbations parallel to \vec{B} . SHIVA implosions have been distorted most seriously by azimuthal perturbations in a pentagonal shape ($k_\theta = 5$). These perturbations have wavelengths on the order of the cylinder radius.

These unstable modes might not be observable here because the number of terms in the trial function needs

to be increased. As the length of our trial velocity function increases, the growth rate estimate increases. The expected parallel instability growth rates may be so small that short trial functions will indeed lead to negative, stable growth rates. Longer trial functions would then be needed to give positive growth rate estimates.

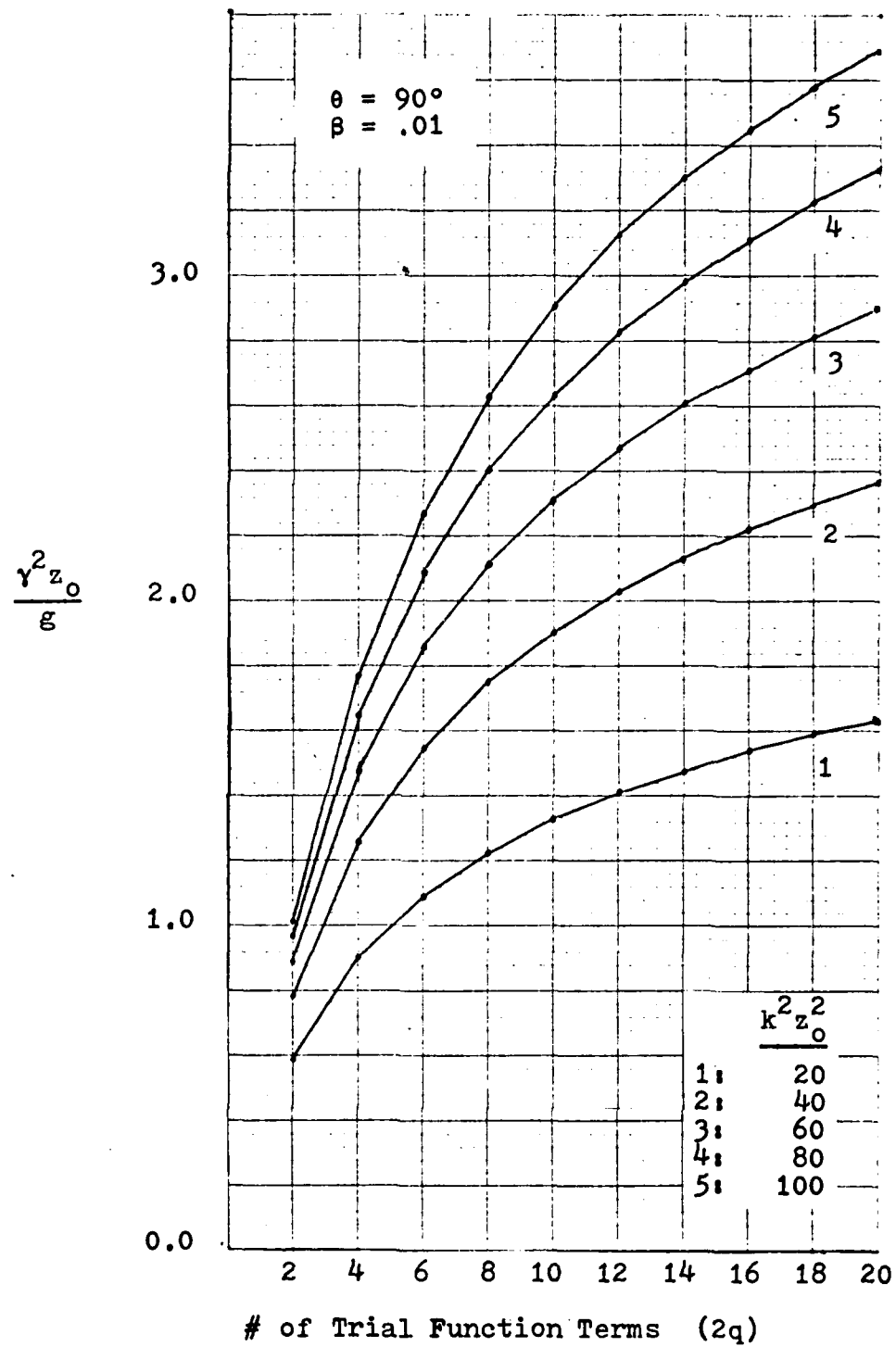


Figure 7. Dimensionless growth rate estimates as a function of trial function length.

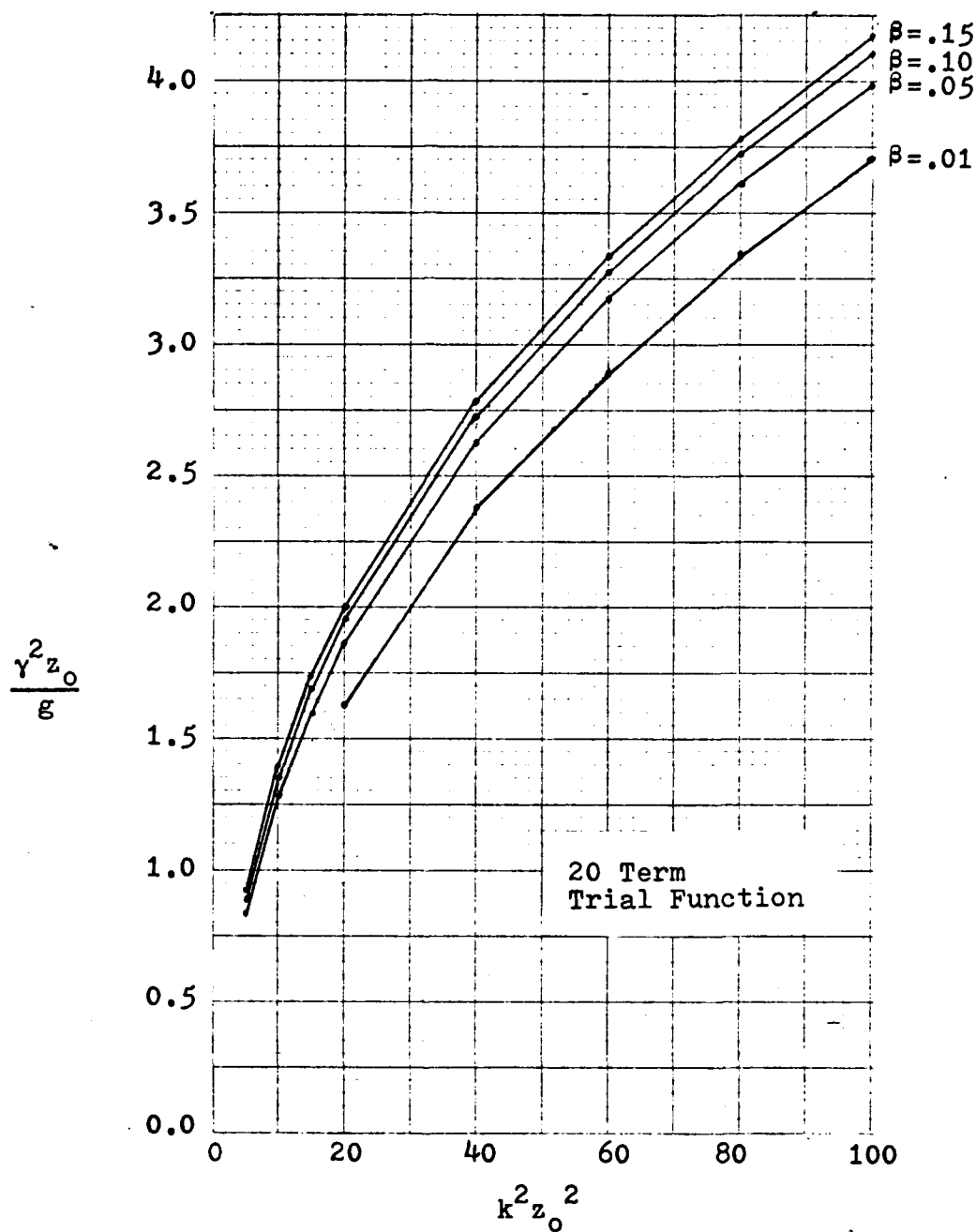


Figure 8. Dimensionless growth rate estimates as a function of perturbation wavenumber for $\theta=90^\circ$.

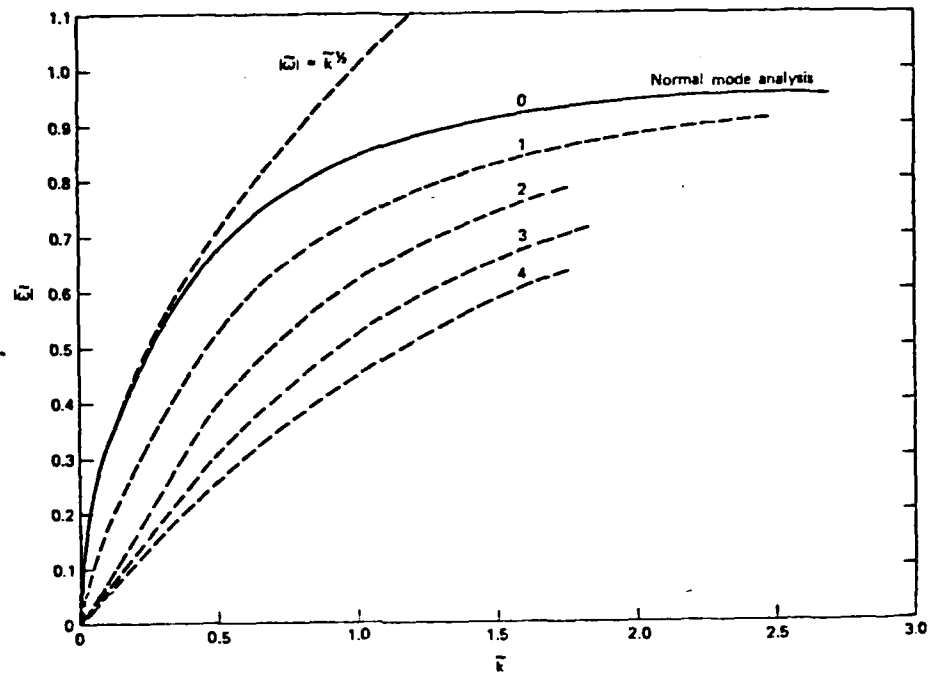


Figure 9. Dispersion relation of Tsai et al for $\theta=90^\circ$. (19) The dimensionless growth rate is plotted as a function of the dimensionless perturbation wavelength.

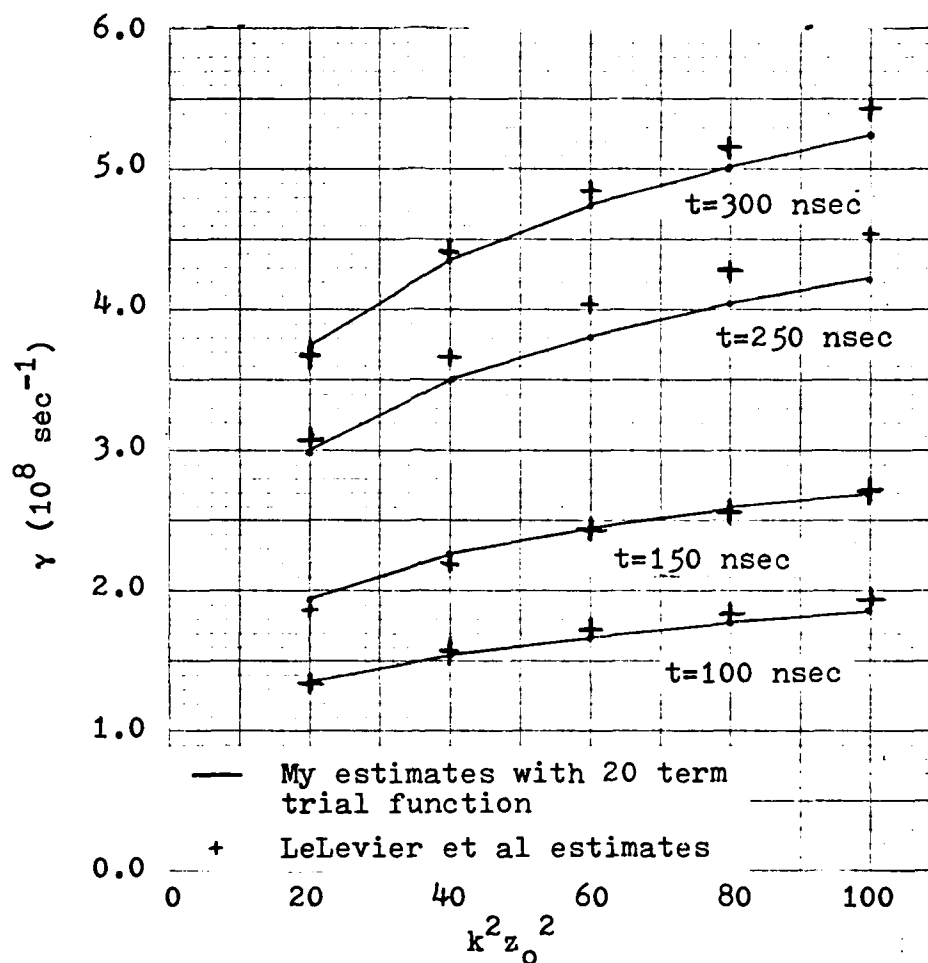


Figure 10. Growth rate estimates as a function of perturbation wavenumber for true SHIVA parameters and $\theta=90^\circ$ compared to LeLevier et al's growth rate (2.29), which assumes an exponential density transition.

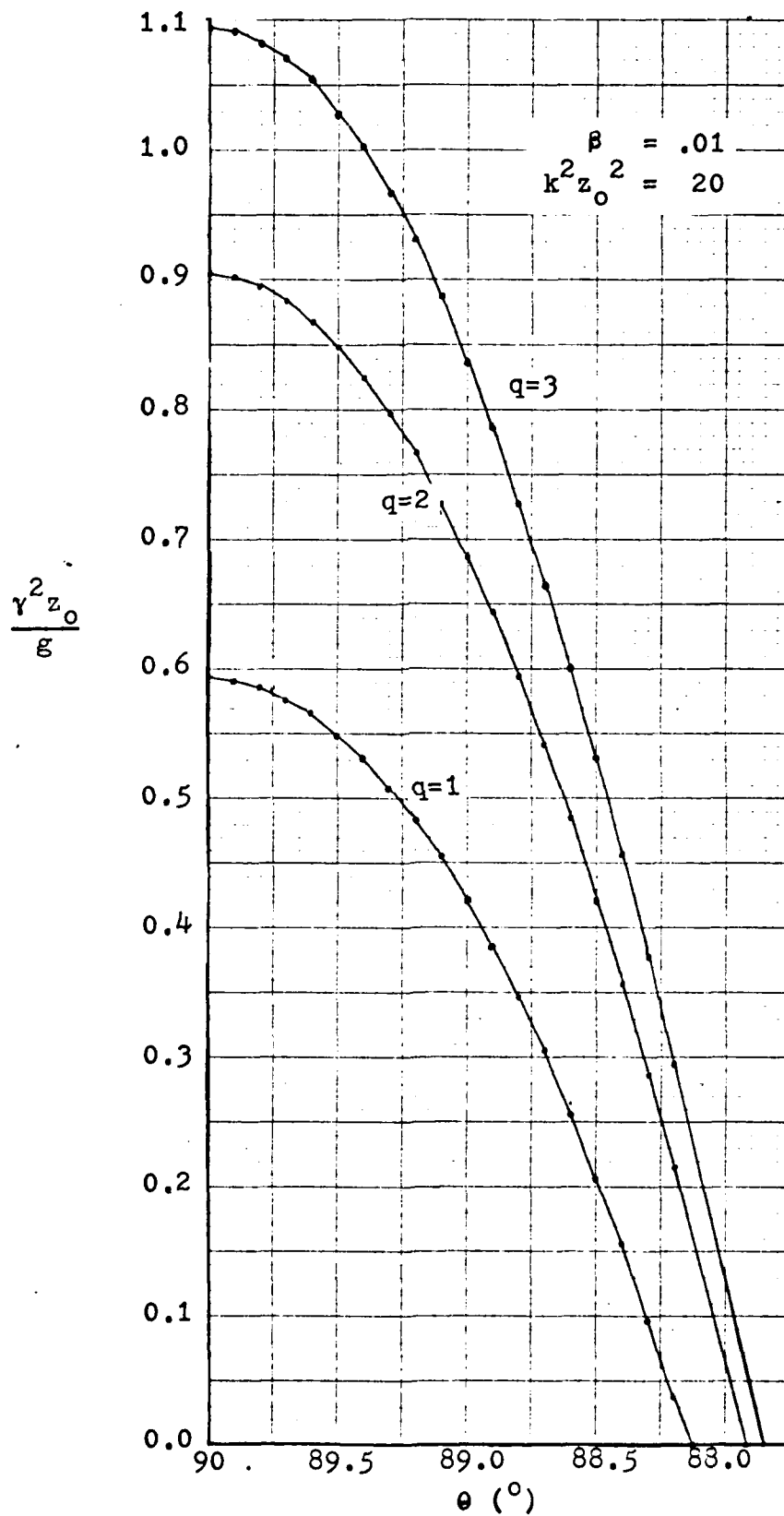


Figure 11. Dimensionless growth rate estimates as a function of θ .

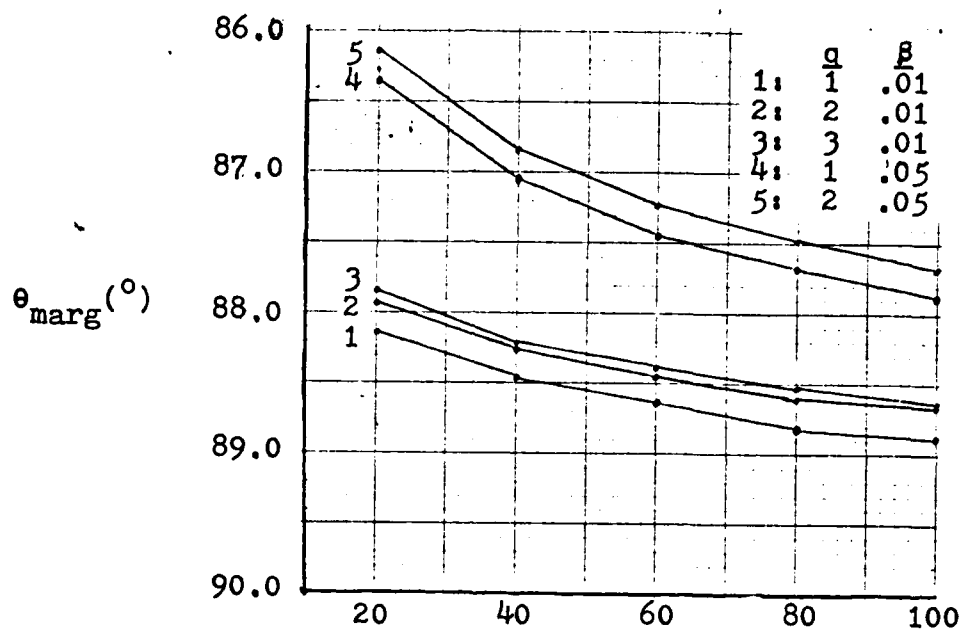


Figure 12. θ_{marg} as a function of perturbation wavenumber.

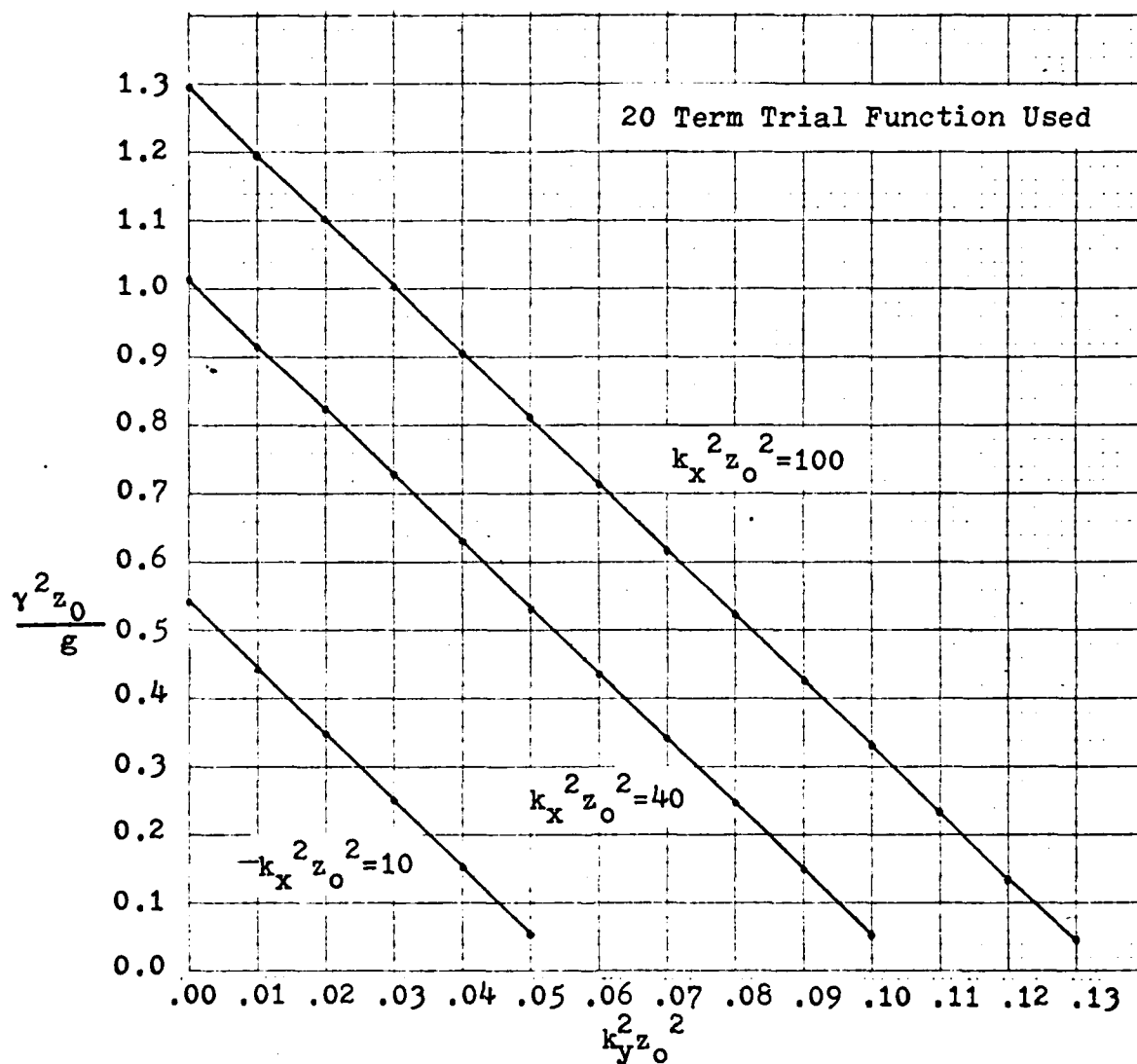


Figure 13. Dimensionless growth rate versus the wavenumber component parallel to the magnetic field. k_x is the component perpendicular to the magnetic field while k_y is the component parallel to the magnetic field.

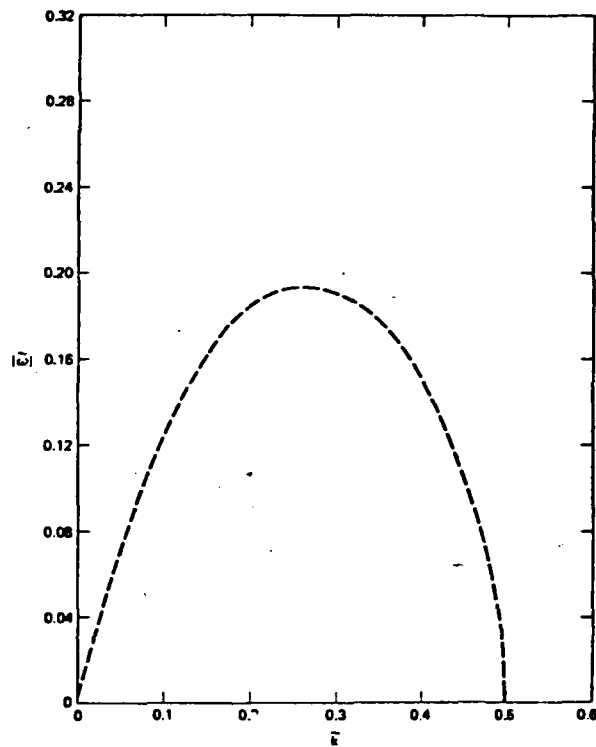


Figure 14. Dispersion relation of Tsai et al for $\theta=0^\circ$. (19)
The dimensionless growth rate is plotted as a function of the dimensionless perturbation wavelength.

TABLE 1

MAGPIE Simulation of 450 ns SHIVA Implosion (9)

<u>Time (ns)</u>	<u>Velocity (cm/μsec)</u>	<u>Radius (cm)</u>	<u>Peak Pressure (Mbar)</u>	<u>Current (MA)</u>
100	- 1.78	7.98	9.56×10^{-4}	11.6
150	- 6.12	7.81	1.13×10^{-3}	15.5
200	-12.17	7.36	1.28×10^{-3}	17.8
250	-19.97	6.56	1.45×10^{-3}	18.24
300	-28.75	5.36	1.80×10^{-3}	17.04
350	-38.12	3.69	2.90×10^{-3}	14.43
400	-48.50	1.53	1.23×10^{-2}	10.33

Initial Foil Mass $\sigma_{in} = 60 \mu\text{g}/\text{cm}^2$ Initial Foil Radius $r_{in} = 8.0 \text{ cm}$

TABLE 2
Derived Variables for 450 ns SHIVA Implosion

<u>Time (ns)</u>	<u>B₀ (MG)</u>	<u>g (cm/μsec²)</u>	<u>λ_{th} (mm)</u>
100	0.291	56.3	.41
150	0.397	107.	.50
200	0.484	169.	.58
250	0.556	250.	.64
300	0.636	400.	.71
350	0.782	879.	.76
400	1.35	6320.	.82

V. Conclusion

A method has been developed to approximate the Rayleigh-Taylor growth rate of an accelerating plasma slab. It has been shown to agree with the analytical results of LeLevier et al (14) for the limiting case $\vec{k} \perp \vec{B}$. This agreement suggests that my choice of a trial velocity function identically equal to zero in the stable region is valid. The behavior of the other limiting case, \vec{k} parallel to \vec{B} , however, is suspect. No unstable modes were found for long wavelengths. This fact may be due to insufficiently long trial velocity functions. If this is not the case, then there may be a more serious problem in this work which brings the presented results (at least for \vec{k} not perpendicular to \vec{B}) into question. As mentioned in the Introduction, the perturbations parallel to \vec{B} are much more interesting than those perpendicular to \vec{B} .

The developed program can also be used to estimate the angle between \vec{k} and \vec{B} at which a particular perturbation wavelength becomes marginally stable. For a given wavelength the instability has been shown to stabilize rapidly as θ decreases from 90° .

The method used here is general and can be used for any density profile with only one contiguous unstable region. The only change necessary is to replace ρ and B in the unevaluated integrals in the first section of Chapter III. Densities with several unstable regions simply

require a trial velocity function which is piecewise defined.

This work can be continued in several ways. First, estimates could be made for a greater variety of parameter values. The present results represent a fairly narrow parameter range. In particular, longer trial velocity functions need to be used with long-wavelength perturbations parallel to B. The expected instabilities might then be observed. Second, the method used to find the solutions of the determinant equation (3.20) -- essentially a binary search method -- might be improved to minimize the number of times the determinant must be evaluated. The current method uses a prohibitive amount of computer time for long trial functions (and therefore large determinants). Third, more accurate density and magnetic field profiles could possibly be found. Hussey and Roderick (10) have presented more accurate profiles which are probably too difficult to work with here. Better approximations to these functions than the ones used here might be possible, however.

Bibliography

1. Ariel, P. D. and Aggarwala, B. D. "The Effect of a General Oblique Magnetic Field on Rayleigh-Taylor Instability", Canadian Journal of Physics, 57 (8), 1094-1117, August 1979.
2. Bateman, Glenn. MHD Instabilities. Cambridge, Mass: MIT Press, 1978.
3. Chandrasekhar, S. Hydrodynamic and Hydromagnetic Stability. Oxford: Clarendon Press, 1961.
4. Degnan, J. H. et al. SHIVA Electromagnetic Implosion X-Ray Source. AFWL-TR-77-252. Kirtland Air Force Base, New Mexico: Air Force Weapons Laboratory, May 1978.
5. Emmons, H. W. et al. "Taylor Instability of Finite Surface Waves", Journal of Fluid Mechanics, 7, 177, 1960.
6. Gelfand, I. M. and Fomin, S. V. Calculus of Variations. Translated and Edited by Silverman, Richard A. Englewood Cliffs, NJ: Prentice-Hall, 1963.
7. Harris, D. L. and Reid, W. H. "On Orthogonal Functions which Satisfy four Boundary Conditions. I. Tables for use in Fourier-type Expansions", Astrophysical Journal Supplement Series, 3, 429-47, 1958.
8. Harris, E. G. "Rayleigh-Taylor Instabilities of a Collapsing Cylindrical Shell in a Magnetic Field", Physics of Fluids, 5(9), 1057-1062, September 1962.
9. Hussey, T. W. Private Communication. Sandia Laboratory, Albuquerque, New Mexico, 1981.
10. Hussey, T. W. and Roderick, Norman F. "Diffusion of Magnetic Field into an Expanding Plasma Shell", Physics of Fluids, 24(7), 1384-5, July 1981.
11. Hussey, T. W. et al. "Scaling of (MHD) Instabilities in Imploding Plasma Liners", Journal of Applied Physics, 51(3), 1452-1463, March 1980.
12. Kanwal, Ram P. Linear Integral Equations. New York: Academic Press. 1971.
13. Kruskal, M. and Schwarzschild, M. "Some Instabilities of a Completely Ionized Plasma", Proc. Roy. Soc., A223, 348-360, 1954.

Bibliography (Contd)

14. LeLevier, R. et al. Effect of a Density Gradient on Taylor Instability. UCRL-4459. Lawrence Livermore Laboratory: Livermore, California, February 1955.
15. Rayleigh, Baron William Strutt. Scientific Papers. New York: Dover. 1964.
16. Reid, W. H. and Harris, D. L. "On Orthogonal Functions which Satisfy Four Boundary Conditions. II. Integrals for Use with Fourier-type Expansions", Astrophysical Journal Supplement Series, 3, 448-52, 448-52, 1958.
17. Roderick, N. F. et al. "Two-dimensional Simulation of the Hydromagnetic Rayleigh-Taylor Instability in an Imploding Foil Plasma", Applied Physics Letters, 32(5), 273-5, 1 March 1978.
18. Taylor, G. I. "The Instability of Liquid Surfaces when Accelerated in a Direction Perpendicular to their Planes. I", Proc. Roy. Soc., A201, 192-6, 1950.
19. Tsai, W. et al. "Rayleigh-Taylor Instabilities of an Accelerating Thin Plasma Slab", Physics of Fluids, 24(9), 1676-81, September 1981.
20. Turchi, Peter J. and Baker, William L. "Generation of High-energy Plasmas by Electromagnetic Implosion", Journal of Applied Physics, 44(11), 4936-45, November 1973.

Appendix A: Cylindrical Sheath Implosion Relations

The basic variables for the implosion of a cylindrical plasma sheath can be related by a series of simple relations. These relations are useful enough to be derived here.

The cylindrical configuration is shown in Figure 15. The first equation relates the magnetic field to the current passing through the sheath. Outside the sheath the field is simply that of a thin wire on axis:

$$B_{\theta} \text{ (G)} = \frac{.2 \text{ I (A)}}{r \text{ (cm)}} \quad (\text{A.1})$$

where r is the radial coordinate.

Equation (A.1) can be used to find the plasma parameter

$$\beta = \frac{P_{\text{mat}}}{P_{\text{mag}}} \quad (\text{A.2})$$

where P_{mat} is the average material pressure and P_{mag} the maximum magnetic pressure in the sheath. We may take

$$P_{\text{mat}} = \frac{1}{2} P_{\text{peak}} \quad (\text{A.3})$$

where P_{peak} is the peak plasma pressure (which is the available variable from computer simulations) and

$$P_m \text{ (Mbar)} = \frac{B_{\theta}^2(r_0)}{8\pi} = \frac{B_0^2 \text{ (MG)}}{8\pi} \quad (\text{A.4})$$

for a cylinder radius r_0 .

The next variable needed is the sheath acceleration g . It is given by the relation

$$g = \frac{B_0^2}{8\pi\sigma} \quad (\text{A.5})$$

where σ is the areal mass density (7:1057). If σ_{in} is the areal mass density of the initial cylindrical foil, then σ is governed by a simple cylindrical convergence relation:

$$\sigma = \frac{\sigma_{in} r_{in}}{r_0} \quad (\text{A.6})$$

where r_{in} is the initial foil radius. Inserting (A.6) into (A.5) then gives

$$g = \frac{B_0^2 r_{in}}{8\pi\sigma_{in} r_0} \quad (\text{A.7})$$

The final relationship will be for the sheath thickness λ_{th} . Hussey and Roderick (9:1385) have developed the approximate relationship

$$\lambda_{th} = \frac{1}{4.51} \left(\frac{\eta t}{\pi} \right)^{\frac{1}{2}} \quad (\text{A.8})$$

where η is the electrical resistivity and t is the time measured from the beginning of the implosion. For lack of better information the resistivity will be assumed constant here.

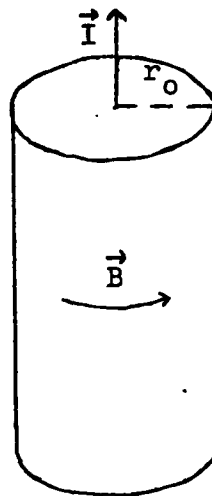


Figure 15. Geometry of a cylindrical implosion.

Appendix B: A Set of Orthonormal Functions

A set of orthonormal functions satisfying the boundary conditions

$$\phi(a) = \phi'(a) = \phi(b) = \phi'(b) = 0 \quad (\text{B.1})$$

for $a < b$ is needed in Chapter III. The functions

$$C_m(u) = \frac{\cosh(\lambda_m u)}{\cosh(\lambda_m/2)} - \frac{\cos(\lambda_m u)}{\cos(\lambda_m/2)} \quad (\text{B.2})$$

and

$$S_m(u) = \frac{\sinh(\mu_m u)}{\sinh(\mu_m/2)} - \frac{\sin(\mu_m u)}{\sin(\mu_m/2)} \quad (\text{B.3})$$

were discussed by Chandrasekhar (3:634-643) and satisfy the equation

$$y^{(iv)} = \alpha^4 y \quad (\text{B.4})$$

with the boundary conditions

$$y(\pm \frac{1}{2}) = y'(\pm \frac{1}{2}) = 0 \quad (\text{B.5})$$

The C's and S's are orthonormal over the interval $(-\frac{1}{2}, \frac{1}{2})$ with eigenvalues given by the solutions of

$$\tanh \frac{\lambda}{2} + \tan \frac{\lambda}{2} = 0 \quad (\text{B.6})$$

and

$$\coth \frac{\mu}{2} - \cot \frac{\mu}{2} = 0 \quad (\text{B.7})$$

The functions C_m and S_m for $m = 1, 2, 3$, and 4 (and their first three derivatives) have been tabulated from $u = 0$ to 0.5 by Harris and Reid (16). Basic indefinite

integrals involving C_m and S_m have been published by Reid and Harris (16). These results allow integrals of the form

$$(\phi_1 | u^n | \phi_2) = \int_{-\frac{1}{2}}^{\frac{1}{2}} \phi_1(u) u^n \phi_2(u) du \quad (B.8)$$

to be calculated simply, with ϕ_1 and ϕ_2 representing C or S and n integer. $(\phi_1 | u^n | \phi_2)$ is integrated by parts q times to leave only integrals of the form $(\phi_1^{(r)} | \phi_2^{(s)})$. The indefinite forms of these integrals are evaluated in Reid and Harris for $r = 0, 1, 2$, and 3. Combining these indefinite integrals with the boundary conditions (B.5) gives a value for the integral (B.8). The explicit forms of C_m and S_m have thus been avoided.

Appendix C: Evaluation of Needed Integrals

All integrals of the form $(\phi_1|f|\phi_2)$ used in Chapter are evaluated here. These integrals fall into two categories: (1) those with $f(u) = 1, u, \text{ or } u^2$ and (2) those with $f(u) = \exp(-au)$. Using the C and S functions of Appendix B as ϕ_1 and ϕ_2 , the first category of integrals can be handled fairly easily using indefinite integrals solved in an article by Reid and Harris (15). The second category of exponential integrals, on the other hand, must be integrated directly using the explicit forms (B.2) and (B.3) of C and S.

As an example of the method used for the first class of integrals, consider the integral $(C_m|u|S_n)$ with $m \neq n$. Integrating by parts,

$$(C_m|u|S_n) = (u/C_m S_n) - \int \int C_m S_n' du \quad (C.1)$$

Reid and Harris list

$$\begin{aligned} (\lambda_m^4 - \mu_n^4) \int C_m S_n' du &= \lambda_m^4 \int C_m S_n' du \\ &\quad - \mu_n^4 \int C_m S_n' du + \int C_m S_n'' du - \int C_m S_n'' du \end{aligned} \quad (C.2)$$

The indefinite integrals on the right hand side of (C.2) are also evaluated by Reid and Harris. Inserting into (C.2) and then (C.1), and remembering that

$$C_m(\pm \frac{1}{2}) = S_m(\pm \frac{1}{2}) = C_m'(\pm \frac{1}{2}) = S_m'(\pm \frac{1}{2}) = 0 \quad (C.3)$$

we have the desired result

$$(C_m' | u | S_n') = \frac{C_m' S_n'' - C_m'' S_n'}{\lambda_m^4 - \mu_n^4} + \frac{4(\lambda_m^4 + \mu_n^4) C_m' S_n'}{(\lambda_m^4 - \mu_n^4)^2} \quad (C.4)$$

where C_m and S_n are evaluated at $u = \frac{1}{2}$. Completing the other integrals from the first class in a similar manner gives (for $m \neq n$)

$$(C_m' | C_m') = -\frac{C_m' C_m''}{2\lambda_m^4} + \lambda_m^2 \tanh^2 \frac{\lambda_m}{2} \quad (C.5)$$

$$(C_m' | C_n') = \frac{2}{\lambda_m^4 - \lambda_n^4} (C_m' C_n'' - C_m'' C_n') \quad (C.6)$$

$$(S_m' | S_m') = \frac{S_m' S_m''}{2\mu_m^4} + \mu_m^2 \coth^2 \frac{\mu_m}{2} \quad (C.7)$$

$$(S_m' | S_n') = \frac{2}{\mu_m^4 - \mu_n^4} (S_m' S_n'' - S_m'' S_n') \quad (C.8)$$

$$(C_m | u | S_m) = \frac{8C_m' S_m''}{(\lambda_m^4 - \mu_m^4)^2} \quad (C.9)$$

$$(C_m | u^2 | C_m) = \frac{1}{12} + \frac{5C_m' C_m''}{4\lambda_m^8} - \frac{5}{2\lambda_m^2} \tanh^2 \frac{\lambda_m}{2} \quad (C.10)$$

$$(C_m | u^2 | C_n) = \frac{8C_m' C_n''}{(\lambda_m^4 - \lambda_n^4)^2} + \frac{4}{(\lambda_m^4 - \lambda_n^4)^3} \{ -(10\lambda_m^4 + 6\lambda_n^4) C_m' C_n'' + (6\lambda_m^4 + 10\lambda_n^4) C_m'' C_n' \} \quad (C.11)$$

$$(S_m | u^2 | S_m) = \frac{1}{12} + \frac{5S_m' S_m''}{4\mu_m^8} - \frac{5}{2\mu_m^2} \coth^2 \frac{\mu_m}{2} \quad (C.12)$$

$$(S_m | u^2 | S_n) = \frac{8S_m' S_n''}{(\mu_m^4 - \mu_n^4)^2}$$

$$+ \frac{4}{(\mu_m^4 - \mu_n^4)^3} \{ -(10\mu_m^4 + 6\mu_n^4) S_m'' S_n''' + (6\mu_m^4 + 10\mu_n^4) S_m''' S_n'' \} \quad (C.13)$$

$$(C_m | u^2 | C_m) = \frac{1}{2} - \frac{C_m'' C_m'''}{8\lambda_m^4} + \frac{\lambda_m^2}{12} \tanh^2 \frac{\lambda_m}{2} + \frac{C_m''^2}{4\lambda_m^4} \quad (C.14)$$

$$(C_m | u^2 | C_n) = \frac{C_m'' C_n''' - C_m''' C_n''}{2(\lambda_m^4 - \lambda_n^4)} + \frac{4(\lambda_m^4 + \lambda_n^4) C_m'' C_n''}{(\lambda_m^4 - \lambda_n^4)^2} \quad (C.15)$$

and

$$(S_m | u^2 | S_n) = \frac{1}{2} - \frac{S_m'' S_n'''}{8\mu_m^4} + \frac{\mu_m^2}{12} \coth^2 \frac{\mu_m}{2} + \frac{S_m''^2}{4\mu_m^4} \quad (C.16)$$

with the C and S functions again evaluated at $u = \frac{1}{2}$.

The second class of exponential integrals are evaluated using the explicit forms of C and S. The results are (with m now allowed to equal n)

$$\begin{aligned} (C_m | e^{-au} | C_n) = & \frac{1}{2 \cosh \frac{\lambda_m}{2} \cosh \frac{\lambda_n}{2}} \left\{ \frac{\sinh \frac{1}{2} (\lambda_m + \lambda_n - a)}{\lambda_m + \lambda_n - a} \right. \\ & + \frac{\sinh \frac{1}{2} (\lambda_m - \lambda_n - a)}{\lambda_m - \lambda_n - a} + \frac{\sinh \frac{1}{2} (\lambda_n - \lambda_m - a)}{\lambda_n - \lambda_m - a} + \left. \frac{\sinh \frac{1}{2} (\lambda_m + \lambda_n + a)}{\lambda_m + \lambda_n + a} \right\} \\ & - \frac{1}{2 \cosh \frac{\lambda_m}{2} \cos \frac{\lambda_n}{2}} \left\{ \frac{2(\lambda_m - a) \cos \frac{\lambda_n}{2} \sinh \frac{\lambda_m - a}{2} + 2\lambda_n \sin \frac{\lambda_n}{2} \cosh \frac{\lambda_m - a}{2}}{\lambda_n^2 + (\lambda_m - a)^2} \right. \\ & + \frac{2(\lambda_m + a) \cos \frac{\lambda_n}{2} \sinh \frac{\lambda_m + a}{2} + 2\lambda_n \sin \frac{\lambda_n}{2} \cosh \frac{\lambda_m + a}{2}}{\lambda_n^2 + (\lambda_m + a)^2} \left. \right\} \\ & + \frac{1}{\cos \frac{\lambda_m}{2} \cos \frac{\lambda_n}{2}} \left\{ \frac{(\lambda_m - \lambda_n) \sin \frac{\lambda_m - \lambda_n}{2} \cosh \frac{a}{2} + \cos \frac{\lambda_m - \lambda_n}{2} \sinh \frac{a}{2}}{a^2 + (\lambda_m - \lambda_n)^2} \right. \\ & + \left. \frac{(\lambda_m + \lambda_n) \sin \frac{\lambda_m + \lambda_n}{2} \cosh \frac{a}{2} + \cos \frac{\lambda_m + \lambda_n}{2} \sinh \frac{a}{2}}{a^2 + (\lambda_m + \lambda_n)^2} \right\} \end{aligned}$$

$$\begin{aligned}
& - \frac{1}{2 \cosh \frac{\lambda_n}{2} \cos \frac{\lambda_m}{2}} \left\{ \frac{2(\lambda_n - a) \cos \frac{\lambda_m}{2} \sinh \frac{\lambda_n - a}{2} + 2\lambda_m \sin \frac{\lambda_m}{2} \cosh \frac{\lambda_n - a}{2}}{\lambda_m^2 + (\lambda_n - a)^2} \right. \\
& + \left. \frac{2(\lambda_n + a) \cos \frac{\lambda_m}{2} \sinh \frac{\lambda_n + a}{2} + 2\lambda_m \sin \frac{\lambda_m}{2} \cosh \frac{\lambda_n + a}{2}}{\lambda_m^2 + (\lambda_n + a)^2} \right\} \quad (C.17)
\end{aligned}$$

$$\begin{aligned}
(S_m | e^{-au} | S_n) = & \frac{1}{2 \sinh \frac{\mu_m}{2} \sinh \frac{\mu_n}{2}} \left\{ \frac{\sinh \frac{1}{2} (\mu_m + \mu_n - a)}{\mu_m + \mu_n - a} \right. \\
& - \frac{\sinh \frac{1}{2} (\mu_m - \mu_n - a)}{\mu_m - \mu_n - a} - \frac{\sinh \frac{1}{2} (\mu_n - \mu_m - a)}{\mu_n - \mu_m - a} + \frac{\sinh \frac{1}{2} (\mu_m + \mu_n + a)}{\mu_m + \mu_n + a} \Big\} \\
& - \frac{1}{2 \sinh \frac{\mu_m}{2} \sin \frac{\mu_n}{2}} \left\{ \frac{2(\mu_m - a) \sin \frac{\mu_n}{2} \cosh \frac{\mu_m - a}{2} - 2\mu_n \cos \frac{\mu_n}{2} \sinh \frac{\mu_m - a}{2}}{\mu_n^2 + (\mu_m - a)^2} \right. \\
& + \frac{2(\mu_m + a) \sin \frac{\mu_n}{2} \cosh \frac{\mu_m + a}{2} - 2\mu_n \cos \frac{\mu_n}{2} \sinh \frac{\mu_m + a}{2}}{\mu_n^2 + (\mu_m + a)^2} \Big\} \\
& + \frac{1}{\sin \frac{\mu_m}{2} \sin \frac{\mu_n}{2}} \left\{ \frac{(\mu_m - \mu_n) \sin \frac{\mu_m - \mu_n}{2} \cosh \frac{a}{2} + a \cos \frac{\mu_m + \mu_n}{2} \sinh \frac{a}{2}}{a^2 + (\mu_m - \mu_n)^2} \right. \\
& - \frac{(\mu_m + \mu_n) \sin \frac{\mu_m + \mu_n}{2} \cosh \frac{a}{2} + a \cos \frac{\mu_m + \mu_n}{2} \sinh \frac{a}{2}}{a^2 + (\mu_m + \mu_n)^2} \Big\} \\
& - \frac{1}{2 \sinh \frac{\mu_n}{2} \sin \frac{\mu_m}{2}} \left\{ \frac{2(\mu_n - a) \sin \frac{\mu_m}{2} \cosh \frac{\mu_n - a}{2} - 2\mu_m \cos \frac{\mu_m}{2} \sinh \frac{\mu_n - a}{2}}{\mu_m^2 + (\mu_n - a)^2} \right. \\
& + \frac{2(\mu_n + a) \sin \frac{\mu_m}{2} \cosh \frac{\mu_n + a}{2} - 2\mu_m \cos \frac{\mu_m}{2} \sinh \frac{\mu_n + a}{2}}{\mu_m^2 + (\mu_n + a)^2} \Big\} \quad (C.18)
\end{aligned}$$

$$\begin{aligned}
(C_m | e^{-au} | S_n) = & \frac{1}{2 \sinh \frac{\mu_n}{2} \cosh \frac{\lambda_m}{2}} \left\{ \frac{\sinh \frac{1}{2} (\lambda_m + \mu_n - a)}{\lambda_m + \mu_n - a} \right. \\
& + \frac{\sinh \frac{1}{2} (\mu_n - \lambda_m - a)}{\mu_n - \lambda_m - a} - \frac{\sinh \frac{1}{2} (\lambda_m - \mu_n - a)}{\lambda_m - \mu_n - a} - \frac{\sinh \frac{1}{2} (\lambda_m + \mu_n + a)}{\lambda_m + \mu_n + a} \Big\} \\
& - \frac{1}{2 \cos \frac{\lambda_m}{2} \sinh \frac{\mu_n}{2}} \left\{ \frac{2(\mu_n - a) \cos \frac{\lambda_m}{2} \sinh \frac{\mu_n - a}{2} + 2\lambda_m \sin \frac{\lambda_m}{2} \cosh \frac{\mu_n - a}{2}}{\lambda_m^2 + (\mu_n - a)^2} \right.
\end{aligned}$$

$$\begin{aligned}
& - \frac{2(\mu_n + a) \cos \frac{\lambda_m}{2} \sinh \frac{\mu_n + a}{2} + 2\lambda_m \sin \frac{\lambda_m}{2} \cosh \frac{\mu_n + a}{2}}{\lambda_m^2 + (\mu_n + a)^2} \} \\
& - \frac{1}{2 \cosh \frac{\lambda_m}{2} \sin \frac{\mu_n}{2}} \left\{ \frac{2(\lambda_m - a) \sin \frac{\mu_n}{2} \cosh \frac{\lambda_m - a}{2} - 2\mu_n \cos \frac{\mu_n}{2} \sinh \frac{\lambda_m - a}{2}}{\mu_n^2 + (\lambda_m - a)^2} \right. \\
& - \frac{2(\lambda_m + a) \sin \frac{\mu_n}{2} \cosh \frac{\lambda_m + a}{2} - 2\mu_m \cos \frac{\mu_n}{2} \sinh \frac{\lambda_m + a}{2}}{\mu_n^2 + (\lambda_m + a)^2} \} \\
& + \frac{1}{\cos \frac{\lambda_m}{2} \sin \frac{\mu_n}{2}} \left\{ \frac{-a \sin \frac{\mu_n - \lambda_m}{2} \cosh \frac{a}{2} + (\mu_n - \lambda_m) \cos \frac{\mu_n - \lambda_m}{2} \sinh \frac{a}{2}}{a^2 + (\mu_n - \lambda_m)^2} \right. \\
& + \frac{-a \sin \frac{\mu_n + \lambda_m}{2} \cosh \frac{a}{2} + (\mu_n + \lambda_m) \cos \frac{\mu_n + \lambda_m}{2} \sinh \frac{a}{2}}{a^2 + (\mu_n + \lambda_m)^2} \} \quad (C.19)
\end{aligned}$$

$$\begin{aligned}
(C_m | e^{-au} | C_n) &= \frac{\lambda_m \lambda_n}{2 \cosh \frac{\lambda_m}{a} \cosh \frac{\lambda_n}{2}} \left\{ \frac{\sinh \frac{1}{2} (\lambda_m + \lambda_n - a)}{\lambda_m + \lambda_n - a} \right. \\
& - \frac{\sinh \frac{1}{2} (\lambda_m - \lambda_n - a)}{\lambda_m - \lambda_n - a} - \frac{\sinh \frac{1}{2} (\lambda_n - \lambda_m - a)}{\lambda_n - \lambda_m - a} + \frac{\sinh \frac{1}{2} (\lambda_m + \lambda_n + a)}{\lambda_m + \lambda_n + a} \} \\
& + \frac{\lambda_m \lambda_n}{2 \cosh \frac{\lambda_m}{2} \cos \frac{\lambda_n}{2}} \left\{ \frac{2(\lambda_m - a) \sin \frac{\lambda_n}{2} \cosh \frac{\lambda_m - a}{2} - 2\lambda_n \cos \frac{\lambda_n}{2} \sinh \frac{\lambda_m - a}{2}}{\lambda_n^2 + (\lambda_m - a)^2} \right. \\
& + \frac{2(\lambda_m + a) \sin \frac{\lambda_n}{2} \cosh \frac{\lambda_m + a}{2} - 2\lambda_n \cos \frac{\lambda_n}{2} \sinh \frac{\lambda_m + a}{2}}{\lambda_n^2 + (\lambda_m + a)^2} \} \\
& + \frac{\lambda_m \lambda_n}{2 \cosh \frac{\lambda_n}{2} \cos \frac{\lambda_m}{2}} \left\{ \frac{2(\lambda_n - a) \sin \frac{\lambda_m}{2} \cosh \frac{\lambda_n - a}{2} - 2\lambda_m \cos \frac{\lambda_m}{2} \sinh \frac{\lambda_n - a}{2}}{\lambda_m^2 + (\lambda_n - a)^2} \right.
\end{aligned}$$

$$\begin{aligned}
& + \frac{2(\lambda_n+a) \sin \frac{\lambda_m}{2} \cosh \frac{\lambda_n+a}{2} - 2\lambda_m \cos \frac{\lambda_m}{2} \sinh \frac{\lambda_n+a}{2}}{\lambda_m^2 + (\lambda_n+a)^2} \\
& + \frac{\lambda_m \lambda_n}{\cos \frac{\lambda_m}{2} \cos \frac{\lambda_n}{2}} \left\{ \frac{(\lambda_m - \lambda_n) \sin \frac{\lambda_m - \lambda_n}{2} \cosh \frac{a}{2} + a \cos \frac{\lambda_m - \lambda_n}{2} \sinh \frac{a}{2}}{a^2 + (\lambda_m - \lambda_n)^2} \right. \\
& - \left. \frac{(\lambda_m + \lambda_n) \sin \frac{\lambda_m + \lambda_n}{2} \cosh \frac{a}{2} + a \cos \frac{\lambda_m + \lambda_n}{2} \sinh \frac{a}{2}}{a^2 + (\lambda_m + \lambda_n)^2} \right\} \quad (C.20)
\end{aligned}$$

$$\begin{aligned}
(S_m | e^{-au} | S_n) &= \frac{\mu_m \mu_n}{2 \sinh \frac{\mu_m}{2} \sinh \frac{\mu_n}{2}} \left\{ \frac{\sinh \frac{1}{2} (\mu_m + \mu_n - a)}{\mu_m + \mu_n - a} \right. \\
& + \frac{\sinh \frac{1}{2} (\mu_m - \mu_n - a)}{\mu_m - \mu_n - a} + \frac{\sinh \frac{1}{2} (\mu_n - \mu_m - a)}{\mu_n - \mu_m - a} + \left. \frac{\sinh \frac{1}{2} (\mu_n + \mu_m + a)}{\mu_m + \mu_n + a} \right\} \\
& - \frac{\mu_m \mu_n}{2 \sinh \frac{\mu_m}{2} \sin \frac{\mu_n}{2}} \left\{ \frac{2(\mu_m - a) \cos \frac{\mu_n}{2} \sinh \frac{\mu_m - a}{2} + 2\mu_n \sin \frac{\mu_n}{2} \cosh \frac{\mu_m - a}{2}}{\mu_n^2 + (\mu_m - a)^2} \right. \\
& + \frac{2(\mu_n + a) \cos \frac{\mu_m}{2} \sinh \frac{\mu_n + a}{2} + 2\mu_m \sin \frac{\mu_m}{2} \cosh \frac{\mu_n + a}{2}}{\mu_m^2 + (\mu_n + a)^2} \\
& - \frac{\mu_m \mu_n}{2 \sinh \frac{\mu_n}{2} \sin \frac{\mu_m}{2}} \left\{ \frac{2(\mu_n - a) \cos \frac{\mu_m}{2} \sinh \frac{\mu_n - a}{2} + 2\mu_m \sin \frac{\mu_m}{2} \cosh \frac{\mu_n - a}{2}}{\mu_m^2 + (\mu_n - a)^2} \right. \\
& + \frac{2(\mu_n + a) \cos \frac{\mu_m}{2} \sinh \frac{\mu_n + a}{2} + 2\mu_m \sin \frac{\mu_m}{2} \cosh \frac{\mu_n + a}{2}}{\mu_m^2 + (\mu_n + a)^2} \\
& + \left. \frac{\mu_m \mu_n}{\sin \frac{\mu_m}{2} \sin \frac{\mu_n}{2}} \left\{ \frac{(\mu_m - \mu_n) \sin \frac{\mu_m - \mu_n}{2} \cosh \frac{a}{2} + a \cos \frac{\mu_m - \mu_n}{2} \sinh \frac{a}{2}}{a^2 + (\mu_m - \mu_n)^2} \right\} \right.
\end{aligned}$$

$$+ \frac{(\mu_m + \mu_n) \sin \frac{\mu_m + \mu_n}{2} \cosh \frac{a}{2} + a \cos \frac{\mu_m + \mu_n}{2} \sinh \frac{a}{2}}{a^2 + (\mu_m + \mu_n)^2} \} \quad (C.21)$$

and

$$\begin{aligned}
(C_m | e^{-au} | S_n) = & \frac{\lambda_m \lambda_n}{2 \cosh \frac{\lambda_m}{2} \sinh \frac{\lambda_n}{2}} \left\{ \frac{\sinh \frac{1}{2} (\mu_n + \mu_m - a)}{\mu_n + \mu_m - a} \right. \\
& + \frac{\sinh \frac{1}{2} (\lambda_m - \mu_n - a)}{\lambda_m - \mu_n - a} - \frac{\sinh \frac{1}{2} (\mu_n - \lambda_m - a)}{\mu_n - \lambda_m - a} - \frac{\sinh \frac{1}{2} (\mu_n + \lambda_m + a)}{\mu_n + \lambda_m + a} \Big\} \\
& - \frac{\lambda_m \mu_n}{2 \sin \frac{\mu_n}{2} \cosh \frac{\lambda_m}{2}} \left\{ \frac{2(\lambda_m - a) \cos \frac{\mu_n}{2} \sinh \frac{\lambda_m - a}{2} + 2\mu_n \sin \frac{\mu_n}{2} \cosh \frac{\lambda_m - a}{2}}{\mu_n^2 + (\lambda_m - a)^2} \right. \\
& - \frac{2(\lambda_m + a) \cos \frac{\mu_n}{2} \sinh \frac{\lambda_m + a}{2} + 2\mu_n \sin \frac{\mu_n}{2} \cosh \frac{\lambda_m + a}{2}}{\mu_n^2 + (\lambda_m + a)^2} \Big\} \\
& + \frac{\lambda_m \mu_n}{2 \cos \frac{\lambda_m}{2} \sinh \frac{\mu_n}{2}} \left\{ \frac{2(\mu_n - a) \sin \frac{\lambda_m}{2} \cosh \frac{\mu_n - a}{2} - 2\lambda_m \cos \frac{\lambda_m}{2} \sinh \frac{\mu_n - a}{2}}{\lambda_m^2 + (\mu_n - a)^2} \right. \\
& - \frac{2(\mu_n + a) \sin \frac{\lambda_m}{2} \cosh \frac{\mu_n + a}{2} - 2\lambda_m \cos \frac{\lambda_m}{2} \sinh \frac{\mu_n + a}{2}}{\lambda_m^2 + (\mu_n + a)^2} \Big\} \\
& - \frac{\lambda_m \mu_n}{\cos \frac{\lambda_m}{2} \sin \frac{\mu_n}{2}} \left\{ \frac{-a \sin \frac{\lambda_m - \mu_n}{2} \cosh \frac{a}{2} + (\lambda_m - \mu_n) \cos \frac{\lambda_m - \mu_n}{2} \sinh \frac{a}{2}}{a^2 + (\lambda_m - \mu_n)^2} \right. \\
& + \frac{-a \sin \frac{\lambda_m + \mu_n}{2} \cosh \frac{a}{2} + (\lambda_m + \mu_n) \cos \frac{\lambda_m + \mu_n}{2} \sinh \frac{a}{2}}{a^2 + (\lambda_m + \mu_n)^2} \Big\} \quad (C.22)
\end{aligned}$$

All integrals listed in this appendix have been verified using a Simpson approximation method for (m, n) equal to $(1, 1)$, $(2, 2)$, and $(1, 2)$.

Vita

Born in Ashiya, Japan in 1958, James has lived in four states and two foreign countries. He entered Indiana University in 1976 and graduated in 1980 with a B.S. in Physics. He then married Susan Arnold. James' initial Air Force assignment was to AFIT in June 1980.

Permanent address: 1575 Southlawn Drive
Fairborn, Ohio 45324

This thesis was typed by Mrs Anna L. Lloyd.

UNCLASSIFIED

SECURITY CLASSIFICATION OF THIS PAGE (When Data Entered)

REPORT DOCUMENTATION PAGE		READ INSTRUCTIONS BEFORE COMPLETING FORM
1. REPORT NUMBER AFIT/GEP/PH/81D-11	2. GOVT ACCESSION NO. AD-A18074	3. RECIPIENT'S CATALOG NUMBER
4. TITLE (and Subtitle) A VARIATIONAL APPROACH TO THE RAYLEIGH-TAYLOR INSTABILITY OF AN ACCELERATING PLASMA SLAB		5. TYPE OF REPORT & PERIOD COVERED MS Thesis
7. AUTHOR(s) JAMES D. TARGOVE 2nd Lt USAF		6. PERFORMING ORG. REPORT NUMBER
9. PERFORMING ORGANIZATION NAME AND ADDRESS		8. CONTRACT OR GRANT NUMBER(s)
11. CONTROLLING OFFICE NAME AND ADDRESS		10. PROGRAM ELEMENT, PROJECT, TASK AREA & WORK UNIT NUMBERS
14. MONITORING AGENCY NAME & ADDRESS (if different from Controlling Office)		12. REPORT DATE December 1981
		13. NUMBER OF PAGES 75
		15. SECURITY CLASS. (of this report) UNCLASSIFIED
		15a. DECLASSIFICATION/DOWNGRADING SCHEDULE
16. DISTRIBUTION STATEMENT (of this Report) Approved for public release; distribution unlimited.		
17. DISTRIBUTION STATEMENT (of the abstract entered in Block 20, if different from Report)		
18. SUPPLEMENTARY NOTES LYNN E. WOLAVER Dean for Research and Professional Development Approved for public release; IAW AFR 190-17 AIR FORCE INSTITUTE OF TECHNOLOGY (AFIT) WRIGHT-PATTERSON AFB, OH 45433 FREDERICK C. LYNCH, Major Director of Public Affairs 23 JUL 1982		
19. KEY WORDS (Continue on reverse side if necessary and identify by block number) Rayleigh-Taylor Instability MHD Instabilities		
20. ABSTRACT (Continue on reverse side if necessary and identify by block number) The growth rate of the hydromagnetic Rayleigh-Taylor instability is approximated here for an accelerating plasma slab. The slab is chosen as a large-radius approximation to an imploding cylindrical foil. A normal mode solution of the MHD equations is assumed, resulting in an integral relation for the instability growth rate. The Rayleigh-Ritz variational method is applied to the relation to estimate the growth rate. A (Continued on Reverse)		

DD FORM 1 JAN 73 1473

EDITION OF 1 NOV 65 IS OBSOLETE

UNCLASSIFIED

SECURITY CLASSIFICATION OF THIS PAGE (When Data Entered)

UNCLASSIFIED

SECURITY CLASSIFICATION OF THIS PAGE(When Data Entered)

BLOCK 20: Abstract (Cont)

linearly decreasing magnetic field is assumed in the slab perpendicular to the acceleration. A corresponding equilibrium mass density profile is then found. Growth rate estimates are then made for these profiles. Calculations are made for perturbation wavevectors perpendicular to the acceleration and at an angle $\theta = 90^\circ$ compare favorably with LeLevier et al's results for a continuous density transition (14). Growth rates for $\theta = 0^\circ$ are stable for all perturbation wavelengths and magnetic field strengths. This contradicts prior results in both slab and cylindrical geometry and suggests an error in this work.

UNCLASSIFIED

SECURITY CLASSIFICATION OF THIS PAGE(When Data Entered)

DATE
FILMED
— 8